We are IntechOpen, the world's leading publisher of Open Access books Built by scientists, for scientists

6,900
Open access books available

185,000
International authors and editors

200M
Downloads

Our authors are among the

154
Countries delivered to

TOP 1%
most cited scientists

12.2%
Contributors from top 500 universities

WEB OF SCIENCE™

Selection of our books indexed in the Book Citation Index in Web of Science™ Core Collection (BKCI)

Interested in publishing with us?
Contact book.department@intechopen.com

Numbers displayed above are based on latest data collected.
For more information visit www.intechopen.com

12

Flow and Mass Transfer inside Networks of Minichannels

Florian Huchet
LCPC
France

1. Introduction

The process miniaturization constitutes a challenge for the Chemical Engineering domain. The particular benefit in term of the increase of the ratio between the transfer surface area and the fluid volume inside microfluidic system is really promising for the conception of efficient apparatus such as microreactors, micromixers and microseparators allowing a better chemical reaction control and heat and mass transfer intensification in order to realize sustainable industrial equipments. On other hand, a proper design of a microstructured platform where miniaturized reactors, mixers and separators are implemented with integrated sensors is crucial for the fabrication of new materials, chemical or bio-chemical products and testing new catalyst and reagent (Gunther & Jensen, 2006). Flow and mass transfer characterization inside these new tools of development and production is fundamental for their optimal design.

Yet, these new pieces of equipment are made in stainless steel integrating about hundreds of microchannels either about several tens of microexchangers. These microstructured exchangers can operate at high pressure and present three-dimensional geometries. Hessel *et al*. (2005) report the order of magnitude of the flow rate in various microstructured reactors. The flow rates range between 10 and 10000 $l.h^{-1}$ and the flow regime is usually transitional or turbulent. In spite of new experimental methods (Sato *et al*., 2003; Natrajan & Christensen, 2007), it remains difficult to measure simultaneously a scalar quantity (concentration, temperature, velocity) at different locations of the microstructured reactors. Thus, a lot of difficulties occur in the prediction of wall transfer phenomena (heat, mass, momentum) in the microstructured reactors in view of their integration in chemical manufacture. A characterization of the flow behaviour and of heat and mass transfer performance is needed in order to develop and improve these microsystems for their application in process engineering. A large number of studies dealing with flow through microsystems of different shapes and flow configurations is available in the literature since a few years. Among them, T-microchannel (Bothe *et al*., 2006) or hydrodynamics focusing (Wu & Nguyen, 2005) are some promising classes of flow configurations for microfluidics apparatus applications. Various complex geometries are usually studied by using numerical approaches or global measurements to characterize transfer phenomena in heat exchangers (Brandner *et al*., 2006) or microreactors (Commenge *et al*., 2004). The flow inside these microreactors or microexhangers are usually in the transitional or turbulent regime and the experimental description of all the hydrodynamics scales become more difficult than in

classical macrodevices. In the mixing research area, the characterization of the mixing scales is nevertheless fundamental for the design and the optimization of the microscale devices. The fluid flow at the microscale level is mainly connected to the characteristics of flow in the transitional and turbulent regimes. The conditions of stationarity, homogeneity and isotropy cannot be assumed in confined turbulent flow in microsystems. Thus, it is of some importance, from both academic and practical points of view, to study confined flow and mixing with particular attention given to the small scale motion. In spite of the recent work dealing with local hydrodynamics analysis inside microchannels, in particular by μPIV (Li and Olsen, 2006), very few paper are dedicated to both hydrodynamics and mixing at the small scales especially in the near-wall vicinity. A high sampling frequency is required to adequately describe a confined turbulent flow characterized by non-Gaussian and high level fluctuations. Recently, it constitutes an important challenge for classical turbulence investigations techniques. (Natrajan & Christensen, 2007, Natrajan *et al*., 2007).

The objective of the experimental research work presented in this chapter is to use several methods in order to characterize flow and mass transfer inside networks composed of crossing minichannels. The cells are some geometric model to study a complex confined flow such as those met in certain mini-heat exchangers or mini-catalytic reactors. The originality is to apply proper experimental methods in order to describe the transfer phenomena at several scales. The global approaches are relevant in the frame of the flow regimes identification and the comparison with other geometries in term of liquid-solid mass transfer performed at three large nickel electrodes and pressure drop measurements. The local approaches are performed in the frame of a multi-scales diagnostic of the flow by PIV (Particle Image Velocimetry) and by using electrochemical microsensors. The electrochemical method constitutes the originality of the used experimental tools. The high potential of electrochemical techniques (Yi *et al*., 2006; Martemianov *et al*., 2007) has recently attracted a significant attention in the microfluidic area due to its ability to detect a large range of species (chemical or biochemical) and the low cost instrumentation compared to optical methods for instance. Integration of multiple microelectrodes allows simultaneous measurements at different locations inside the microexchanger. The electrodiffusion probes are used for the mapping of wall shear rates in the flow cell. An array of 39 microelectrodes allows us to characterize the flow regimes, longitudinal and lateral evolutions of the flow structures and flow behaviour at the channels crossings. In other hand, the use of the electrochemical microsensors method is also adapted to the characterization of the mixing state in different geometries of minireactor composed of networks of minichannels.

Thus, this chapter is organized in several sections:

- the next section is dedicated to the presentation of the electrochemical diagnostics based on the condition of the diffusional limitation at the wall microprobes. Two methods allowing the assessment of the instantaneous wall shear rate determination are compared by using an adapted signal processing tools,
- the third section is dedicated to the materials and the calibration methods with a special attention given to the experimental cell composed of a network of crossing minichannel.
- the fourth section presents the local flow results obtained using PIV measurements and the electrodiffusion diagnostics,
- the fifth section deals with the global characterization by using liquid-solid mass transfer and pressure drop measurements,
- the sixth section is dedicated to the mixing performance characterization inside two differents networks of minichannels,
- conclusion and outlooks are finally drawn.

2. Electrochemical method and post-processing tools

2.1 Electrodiffusion technique

The technique is based on the wall shear rate measurement (Hanratty & Campbel, 1983) consisting in using mass transfer probes flush-mounted in the wall. A potential difference is applied between the microprobes acting as cathodes and a large area anode. A fast electrochemical reduction reaction takes place at the microprobes surface allowing the diffusion boundary layer development as drawn in figure 1.

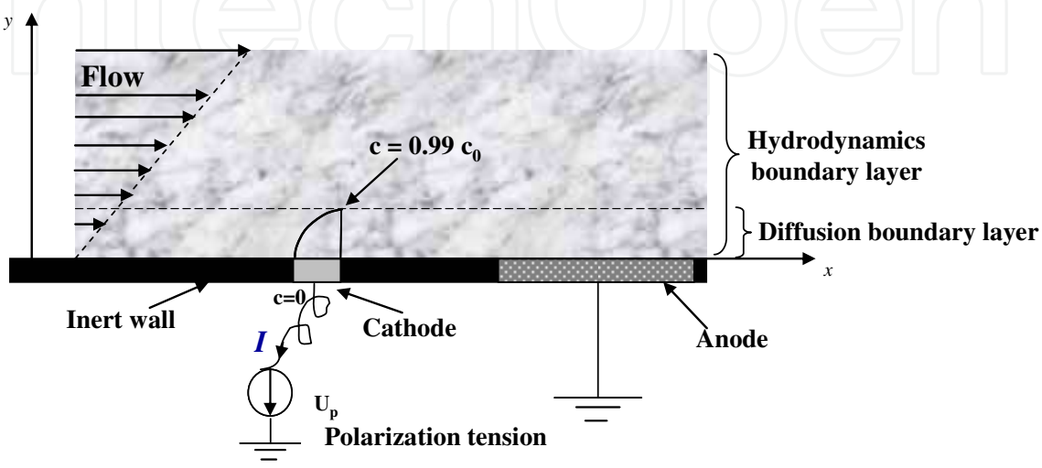

Fig. 1. Electrochemical method principle

The electrochemical reaction employed in the frame of our work is the reduction of ferricyanide ions on a circular platinum cathode:

$$Fe(CN)_6^{3-} + e^- \rightarrow Fe(CN)_6^{4-} \tag{1}$$

The principle involves the measurement of a current under diffusional limiting conditions at the microprobes in such a way that the reaction rate is diffusion-controlled through the mass transfer boundary layer, δ_d, and that the ionic migration can be neglected due to the presence of a supporting electrolyte. The measured intensity varies with the applied voltage between the anode and the cathode until it reaches a constant value, I_{lim}, corresponding to the limiting diffusion conditions. The mass transfer coefficient, k, can then be calculated by the Faraday's expression:

$$k = I_{lim} / v_e \Im A c_0 \tag{2}$$

where v_e is the number of electrons involved in the red-ox reaction, $\Im$ is the Faraday's constant, A is the surface area of the microelectrode and c_0 is the bulk concentration of the reacting species.

In the case of large active surface of the electrode, the measured mean current correspond to the global mass transfer at the wall, k_{mt}.

By working with microelectrodes, the mean measured limiting current is controlled locally by convective diffusion and the well-known Lévêque formula (Lévêque, 1928) can be applied to determine the mean wall shear rate, $\bar{s}$. The stationary equation has been solved (Reiss & Hanratty, 1963) for a circular microelectrode:

$$\bar{s} = 3.22\left(\bar{I}_{lim} / v_e \Im c_0 d_e^{5/3} D^{2/3}\right)^3 \quad (3)$$

where d_e is the diameter of the circular electrode, and D is the diffusion coefficient of the active species in the solution.

The analytical quasi-steady state interpretation solution of the measured current correctly describes the time response of the mass transfer rates, and the instantaneous wall shear rate, $s_q(t)$, can be related to the instantaneous mass transfer rates by the same equation as for steady flow (equation 2):

$$s_q(t) = 3.22(v_e \Im c_0)^{-3} D^{-2} d_e^{-5} I_{lim}^3(t) \quad (4)$$

For high frequency fluctuations of the wall shear rate the filtering effect of the mass boundary layer damps the fluctuations of the mass transfer rate and the quasi-steady solution is not yet representative. The cut-off frequency under which the quasi-steady-state can be considered to be valid is rather low owing to the large value of the Schmidt number in the electrolyte (Sc≈1700). Two methods are currently used in order to evaluate the wall shear rate fluctuations.

From the power spectra density (PSD) of the instantaneous current fluctuations, $W_{ii}(f)$, the transfer function, $H(f)$, allows the assessment to the power spectra density of the wall shear rate fluctuations, $W_{ss}(f)$. Thus, the frequency response of the electrochemical probes is taken into account to restore the shear rate fluctuations spectrum from the current fluctuations one by using the following relationship:

$$W_{ss}(f) = W_{ii}(f) / |H(f)| \quad (5)$$

A correct use of equation 12 supposes two conditions:

i. the transfer function must be accurately known in the whole frequency range,
ii. the homogeneity condition with time-depending fluctuations and the average value must be uniform over the whole probe surface.

Concerning circular probes, several forms of $|H(f)|$ have been the objective of several studies (Nakoriakov *et al*., 1986, Deslouis et al., 1990) that we have presently applied to the limiting current obtained after applying Fourier's transform. This function allows the determination of the wall shear stress dynamics.

The second method, based on the Sobolik's correction (Sobolik *et al*., 1987), takes into account the calculation of the wall shear stress time-evolution.

2.2 Sobolik correction

This method is based on a correction with respect to the probe dynamic behaviour by using the diffusion-convection equation solution (Sobolik *et al*., 1987). These authors solved the mass balance equation assuming that the concentration field is a similar function of three variables:

$$c(x, y, t) = c_0 f(\eta) \quad (6)$$

$$\eta = y f(t)^{1/3} / \delta_d(x) \quad (7)$$

where *f(t)* is a general time function which takes into account the time shifting of the wall shear rate. The resolution of the diffusion-convection equation in the whole mass boundary layer leads to a general expression of the time history of the wall shear rate, $s(t)$:

$$s(t) = s_q(t) + \frac{2}{3} t_0 \left(\frac{\partial s_q}{\partial t}\right) \tag{8}$$

where t_0 is the characteristic time of the probe defined as a dynamic behaviour parameter of the electrodiffusion probe:

$$t_0(t) = 0.426 \; d_e^{2/3} D^{-1/3} s_q(t) \tag{9}$$

This relationship was used by several authors in different flow configurations (Labraga *et al*., 2002 ; Tihon *et al*., 2003) who found it relevant in unsteady flow conditions, even by comparison with inverse method (Rehimi *et al*., 2006).

2.3 Power spectra density assessments

The comparison of the electrochemical transfer function and the corrected solution (Sobolik et al., 1987) can be made using a frequential representation of the signals. The procedure of the signal treatment is given in the present under-section according to the methodology presented in figure 2.

It corresponds to the steps generally applied in order to obtain the experimental characterization of a turbulent flow from passive scalars or from one of two components of the velocity.

The unsteady variations of the current measured from the microelectrodes correspond to the fluctuations of the concentration of the active species into the diffusive boundary layer. There are strongly connected to the flow fluctuations developed into and outside the hydrodynamical boundary layer. The recording of a random signal such as the current needs a one-dimensional Fourier transform in order to obtain the repartition of the energy in the frequencies space. It gives a physical sense to the temporal signal that appears as a noise. The present methodology is inspired from literature (Max, 1985). The first step consists in extracting the fluctuating value, i(t), of the recorded signal, $I_{lim}(t)$, defined by :

$$I_{lim}(t) = \overline{I_{lim}} + i(t) \tag{10}$$

The resulting signal is divided in several blocs, N, having the same number of points, N_e. Each bloc recovers the half part of the previous one. Each part of the signal, $i(t)_N$, is treated independently. This averaging method allows to remove perturbations (as ambient noise or electromagnetism wave) and to conserve the physical phenomenon representation. The number of points, N_e, of each bloc depends on the temporal resolution of the studied phenomenon. The sampling frequency is adjusted as a function of the turbulence level in order to describe all the physical information in the various sub-ranges of the spectra: from the scale of energy containing eddies to the smallest scale depending on the ratio of diffusivities, the Schmidt number.

In the other hand, each bloc is multiplied by a temporal window with the same size N_e. This function allows eliminating of the lobe phenomenon which occurs when a Fourier transform is applied to a finite signal.

This truncation effect can be reduced by several kinds of windows (Hanning, Blackman). Among them, the Hanning's window has been retained, which is defined by:

$$F_{ha}(t) = 0{,}5 \times (1 + \cos\frac{\pi t}{N_p}) \tag{11}$$

The power spectral density of the current, $W_{ii}(t)_N$, is obtained by discrete Fourier transform of the focused parts of the signal and their integration gives rise to the DSP, W_{ii} :

$$W_{ii}^{i} = \int_{0}^{N_e} (i(t)_N \times F_{ha}(t)) \times \exp(-j2\pi ft)dt \tag{12}$$

$$W_{ii} = \frac{\sum_{i=1}^{N} W_{ii}^{i}}{N} \tag{13}$$

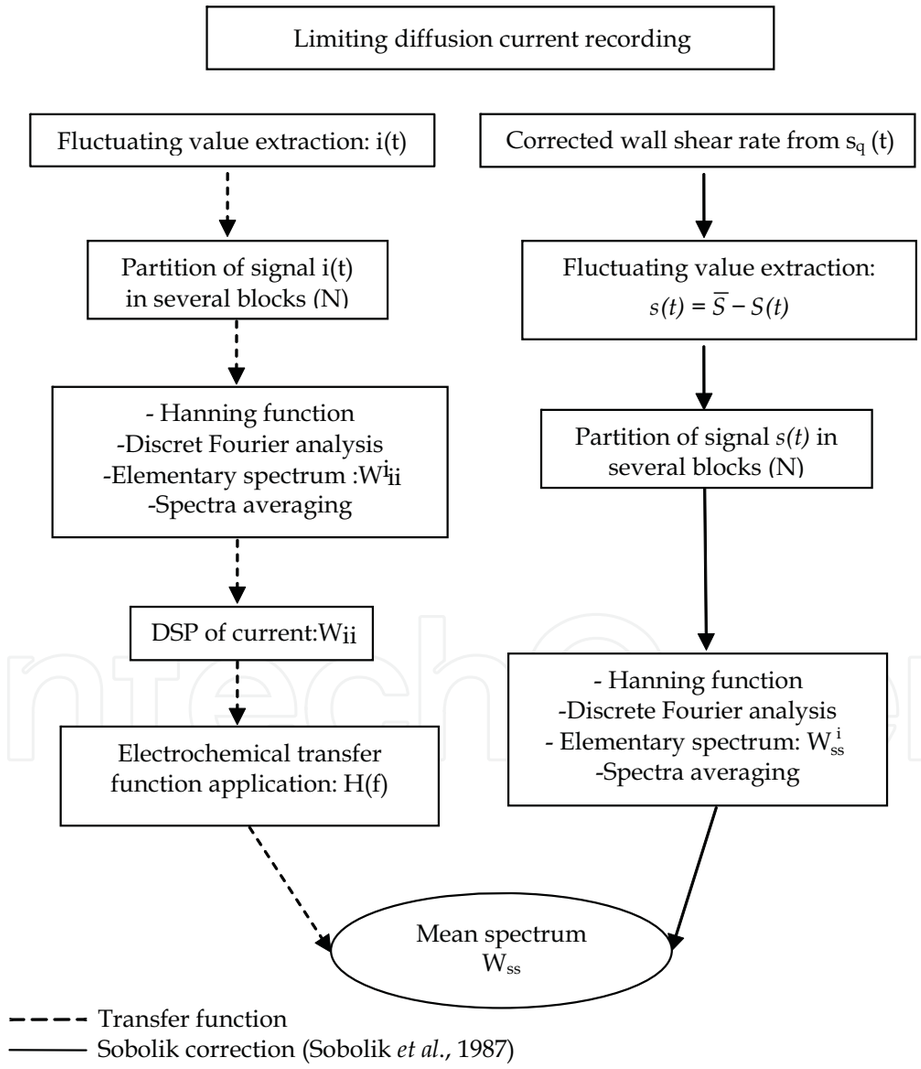

Fig. 2. Different steps of the signal processing

3. Materials & calibration methods

3.1 Experimental set-up

The experimental cell is shown in Fig. 3. It is made of Altuglas and composed of crossing minichannels. The individual square-cross sections of the channels (1.5 mm in side) intersect at right angles. The whole test section has a length of H=105 mm and a width of L=52 mm. At the inlet, there is a calming section containing glass spheres 2 mm in diameter, which allow better distribution of the fluid. Two bottom plates were successively used in order to perform two measurements techniques. One includes thirty-nine circular platinum microelectrodes flush-mounted to the wall allowing an electrodiffusion diagnostics of the wall-flow. The second one is a transparent plate required for the visualization in the frame of PIV measurements.

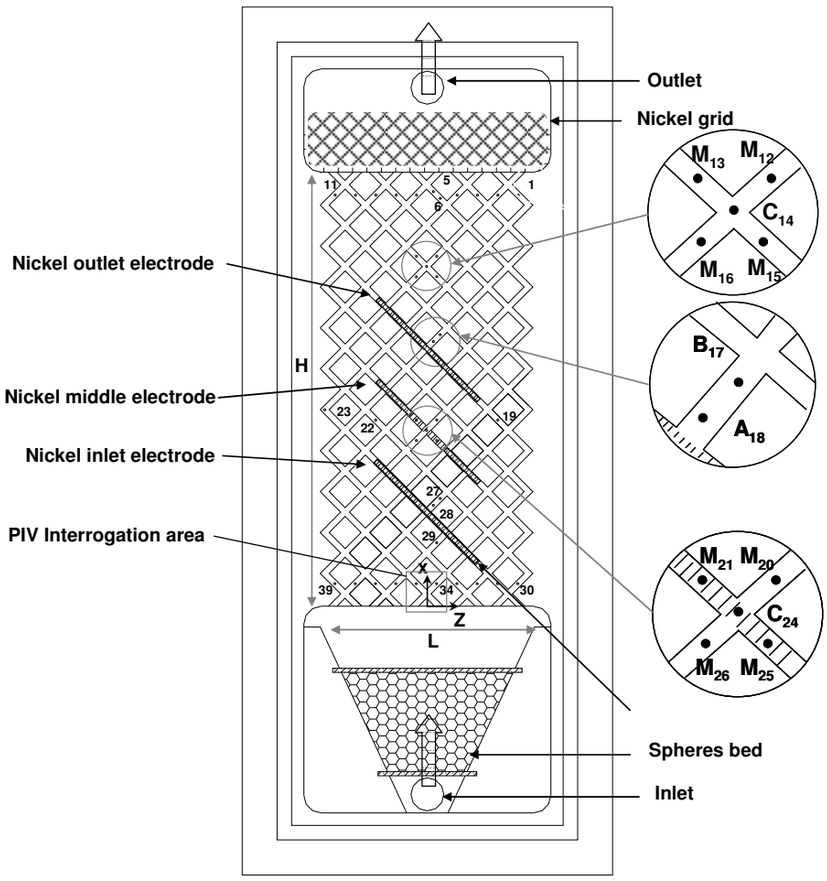

Fig. 3. Scheme of the experimental cell

The microelectrodes have a nominal diameter of 0.25 mm working as cathodes. The anode is made of a nickel grid located at the cell outlet section. As seen in Fig.3, the microelectrodes are numbered from right to left and from top to bottom. The microelectrode positions with respect to the individual minichannel sections are designated with four different labels: M (at the middle of a channel section), A (just after channel crossing), B (just before crossing), and C (at the center of a channel crossing). Two dimensionless parameters are used to

determine the position of each probe inside the network of minichannels. The axial position is represented by the parameter $X=x/H$ and the lateral one by $Z=2z/L$. The large nickel electrodes (strips with dimensions of $d_h \times l_e = 1.5 \times 3.65$ mm) are placed at three flow cell positions in order to study the global mass transfer inside the flow cell. The exact surface area of each electrode is obtained by image analysis.

A suitable electrochemical system is provided by an addition of 0.025 M equimolar potassium ferro/ferricyanide and 0.05 M potassium sulphate into water. The polarization voltage of -0.8 V is applied to ensure limiting diffusion current measuring conditions. A home-built electrodiffusion analyser is used to set the polarization voltage to the microelectrodes, to convert the measured currents into voltages and to amplify the resulting signals. A PC computer controlled the analyser operation and data recording. Data records (ranging from 30000 to 80000 samples, depending on the Reynolds number value) from eight current signals are provided at a sampling frequency ranging from 3 kHz to 8 kHz.

The experiments were performed at Reynolds numbers Re ranged from 50 to 3000. The Reynolds number, $Re=u_c.d_h/v$, is based on the channel hydraulic diameter, d_h, v being the kinematic viscosity of the working fluid and the mean velocity inside individual channel sections u_c is defined by:

$$u_c = \frac{Q_0}{nA_c} \tag{14}$$

where n is the number of minichannels at the inlet and at the outlet (n=10), A_c, the section of an individual minichannel. By assuming a uniform repartition of the flow rate at inlet and outlet, the flow rate inside the minichannel, Q_c, is calculated from the total flow rate, Q_0, by:

$$Q_c = \frac{Q_0}{n} \tag{15}$$

All measurements have been carried out at the room temperature.

3.2 Calibration method

The electrochemical probes are made from a platinum wire 250 µm in diameter, but the real active surface area at which mass transfer occurs can be different of the geometrical one due to the manufacturing process. Thus, the calibration technique used in this work is based on the study of the transient response of the microelectrode to polarization switch-on (Sobolik *et al.*, 1998). This current response is described by the well-known solution of unsteady diffusion in stagnant fluid:

$$I(t) = \tfrac{1}{4} \nu_e F C_0 \pi d_e^2 \sqrt{D/\pi t} \tag{16}$$

with D, the molecular diffusion coefficient of the reacting species.

The transient current measured consecutively to a voltage step is used to determine the individual effective diameter, d_e, of each microelectrode. In spite of shape deformation during the process of microelectrode fabrication, the effective diameter values is found equal to 0.25 mm with a mean deviation of 0.01 mm for ten repetitions of the calibration. These values is found to be close to the platinum wire nominal diameter as shown in the table 1.

Electrode	**1**	**2**	**3**	**4**	**5**	**6**	**7**	**8**	**9**	**10**
d_e (mm)	0,251	0,249	0,252	0,262	0,267	0,275	0,298	0,250	0,267	0,288
Electrode	**11**	**12**	**13**	**14**	**15**	**16**	**17**	**18**	**19**	**20**
d_e (mm)	0,242	0,245	0,240	0,229	0,253	0,268	0,246	0,225	0,291	0,270
Electrode	**21**	**22**	**23**	**24**	**25**	**26**	**27**	**28**	**29**	**30**
d_e (mm)	0,246	0,258	0,256	0,256	0,241	0,282	0,289	0,256	0,264	0,230
Electrode	**31**	**32**	**33**	**34**	**35**	**36**	**37**	**38**	**39**	
d_e (mm)	0,243	0,249	0,250	0,258	0,254	0,266	0,224	0,262	0,242	

Table 1. Recapitulative of the microelectrode diameter

3.3 Molecular diffusion coefficient

The measurements of the diffusion coefficient, D, of the ferricyanide ions inside the working solution were obtained by the classical Levich method (Coeuret & Stork, 1984) which uses a rotating disc electrode system. The advantage of this device deals with the possibility to use a working electrode with a well defined surface area (in our experiments $S = 3.14 \times 10^{-6}$ m²) and to work with small electrolyte volume in well-controlled hydrodynamic conditions. The diffusion coefficient, D, is obtained from the experimental dependence of the limiting diffusion current, I_L, versus the angular rotation speed of the disc, ω:

$$I_L = 0.621 \nu_e C_0 F S D^{2/3} \nu^{-1/6} \omega^{1/2} \tag{17}$$

where v is the kinematic viscosity of the solution.

A set of experiments performed in a large range of temperature values (285 <T(K)<305) are significant in order to check the Stokes-Einstein relationship between dynamic viscosity, diffusivity and absolute temperature :

$$\frac{\mu D}{T} \cong 2{,}18 \times 10^{-15} \mathrm{m}^2.\mathrm{Pa}.\mathrm{K}^{-1} \tag{18}$$

4. Local flow diagnostics

4.1 PIV measurements

The experimental testing bench included a laser (Nd-Yag, 15 Hz, 120 mJ), a double image recorder camera (Kodak megaplus ES 1.0, 1008 × 1016 pixels) which is joined to a 28 mm lens and three macroscopic sleeves. The dedicated processor (PIV 2100) and Flowmanager V 4.5 software is used to perform the calculations of the flow fields using the cross-correlation method. The seeding material is spherical polyamide particles from Dantec (density = 1.03, d_P=20 μm). Interrogation areas are squares of 32 × 32 pixels. The laser, the CCD camera and

the cell are placed on an individual moving system. The water pump are preceded by a mixer and the working cell is placed on a stiff table mounted on slender screws in order to reduce the vibrations induced by the pump. Micrometric moving systems are used to align the laser beam in the fluid plane and to accurately focalize the camera on the measurement plane. By moving the laser, the thickness of the laser sheet crossing the network cell has a minimum value less than 1 mm.

In those conditions, the magnification ratio is closed to 1:1 and the investigated visualisation field measured is 1 cm × 1 cm. The field depth of the image is measured by a diffraction grating and is approximately equal to 300 µm. The seeding concentration is adjusted to get between 5 and 10 particles in each interrogation window. The statistical averaging of the data was performed on a series of 1000 instantaneous velocity fields and the statistical convergence is checked on mean velocity, and second-order moments of fluctuating velocity.

The measurements are focused on eight zones corresponding to the location of the electrochemical probes. The experiments are performed at Reynolds number, *Re*, ranged from 145 to 1620. The results are limited to one zone at the inlet of the network in order to present the PIV results. The whole of the results are available in the publication of Huchet *et al*. (2008)a.

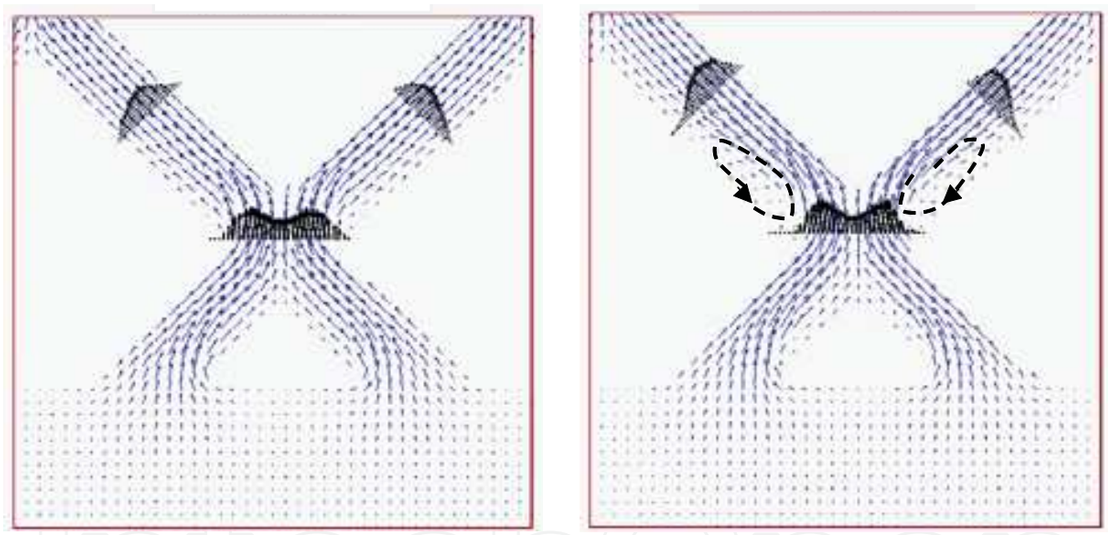

Re= 144 Re=1270

Fig. 4. Velocity profiles and mean flow fields in zone 1 at the inlet of the network for two Reynolds numbers.

The results of mean flow fields are presented in Fig. 4 at low Reynolds number (*Re* = 144) and higher Re value (Re=1270) at the inlet. For Re=144, no instability and no significant detachment appear after the crossing channels. Three velocity profiles are plotted, one of them is located at the crossing and is characterized by two peaks corresponding to the laminar velocity profile of each incoming channel. The velocity increases on both sides of the crossing centre and depicts the symmetrical distribution of the flow in the two outlet branches. The mean velocity at the crossing junction is found 1.7 times higher than in the outlet branches. Normally, the ratio between the velocity at the crossing section and the incoming channel velocity should be $\sqrt{2}$. The lack of resolution in the near wall region tends to overestimate the experimental values.

For *Re*=1270, and as previously observed, the velocity decreases in the crossing centre. A large recirculation zone is observed on the opposite side of the rear location of the crossing and is associated to a preferential flow which presents more important momentum transfer at this location. The recirculation extends over half of the length between two successive crossings and covers half of its width. The velocity fields are quite similar in each channel after the crossing and the flow structure is non-established after the impact of the two incident streams in comparison to the parabolic profile obtained in fully developed laminar flow.

4.2 Wall shear rate fluctuations measurements from microelectrodes
4.2.1 Power spectrum density analysis
4.2.1.1 PSD of the current : W_{ii}

Figure 5 shows the PSD of the current, W_{ii}, for a large range of Reynolds numbers (317<Re<3535) at three different positions in the network either at the inlet (electrode M34), at the middle (A28) and close the outlet (M15) of the system.

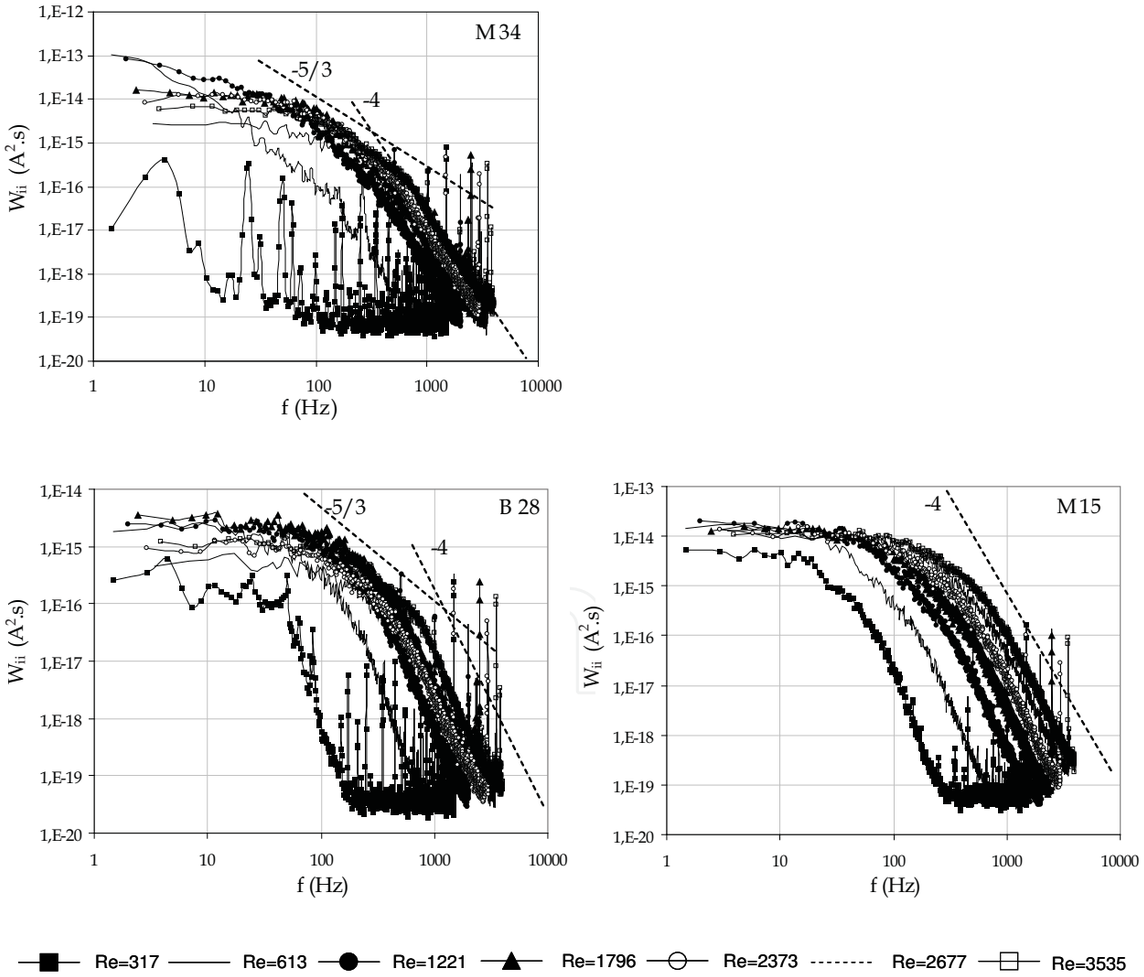

Fig. 5. PSD of the limiting current fluctuations for three electrodes (M_{34}, B_{28}, M_{15}) at different Reynolds numbers.

As previously proven by Tennekes & Lumley (1972), the cascades of the spectra correspond quite well to the standard concentration spectra of the electrochemical species dynamically mixed in the diffusion boundary layer. For the electrodes located in the non-established flow area (M34 to A28), the low frequency part of the spectra gives rise to a decrease until 30 Hz. From 30 Hz to 130 Hz, the logarithmic trends are characterized by a slope equal to $f^{-5/3}$ which corresponds to the inertial-convective sub-range where the large scale structures govern the transport of the passive scalar. Above f=130 Hz the spectra fall-down with a slope equal to f^{-4}. For M15 location, where the flow is fully developed, the spectra are characterized by a low frequency plateau and the downward slope reaches f^{-4} at a frequency (20<f(Hz)<120) which is increasing with Re.

4.2.1.2 PSD of the wall shear rate : W_{ss}

The PSD of the wall shear rate fluctuations obtained from using the electrochemical transfer function are presented in figure 6 and compared with the PSD calculated from the wall shear rate fluctuations from the Sobolik correction (equation 8).

Each spectrum is characterized by a low frequency plateau and a decrease in the high frequency area. The slope in this last part of the spectra differs according to the position of the probe in the network. The value of the slope depends on the nature of the flow. It has to be noticed in the present case that the first hypothesis is not respected. The transfer function does not manage to represent properly the whole range of the fluctuations as a cut-off frequency appears in each spectrum (500<f(Hz)<1500). Therefore, the linearization theory of the transfer function is not yet valid and the direct correction of the electrochemical signals seems to be a more attractive method to solve the issue of the dynamic behaviour of the electrochemical probe. The shape of the PSD of the corrected wall shear rate is similar to that calculated by the transfer function in the range of frequency corresponding to the intermediate and large flow structures (1<f(Hz)<1000). Above a frequency value equal to f≈1500Hz, the PSD of the corrected wall shear rate gives some information in the dissipative area of the spectra, which are impossible to obtain with the transfer function method.

It may be noticed that the level of the wall shear rate fluctuations calculated using the transfer function remains correct since this part of the spectra does not influence the integrate value of the PSD (Huchet *et al*., 2007). Nevertheless, it is important to select the corrected method of Sobolik *et al*. (1987) to analyse mixing phenomenon from the electrochemical method application. The reason is that the flow structures associated to the micromixing phenomena which allow the best conditions for the reaction are located in the dissipative part of the spectra. Thus, we propose to apply in the following section this method for the characterization of the flow regimes by spectra integration to access the fluctuating rate of the wall shear rate:

$$FR = \sqrt{\overline{s'^2}} \Big/ \bar{s} = \sqrt{\int W_{ss} df} \Big/ \bar{s} \ , \tag{19}$$

with

$$s(t) = \bar{s} + s'(t) \tag{20}$$

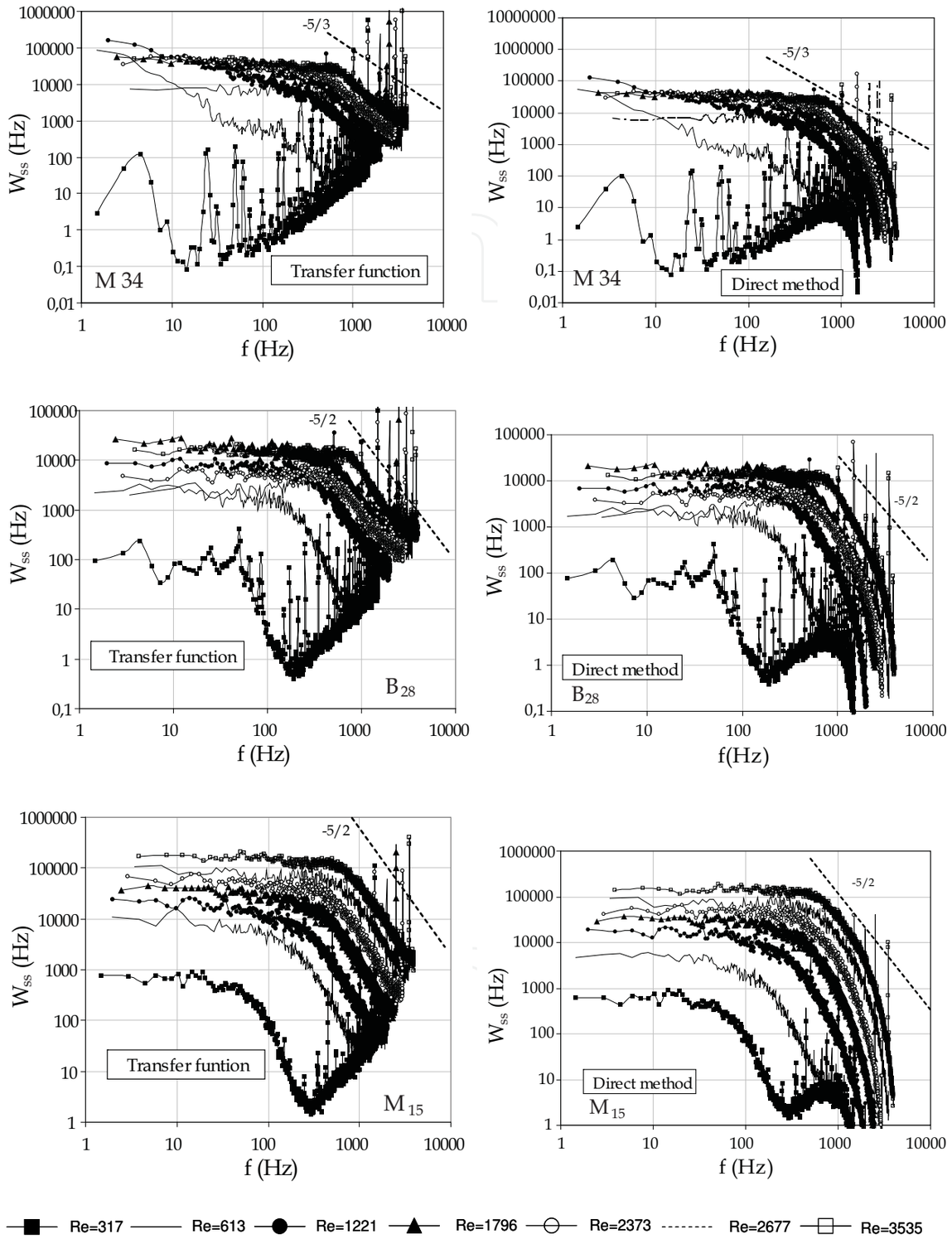

Fig. 6. Comparison of the PSD of the wall shear rate fluctuations between transfer function method and Sobolik's solution (direct solution) for three working microelectrodes and several Reynolds numbers.

4.2.2 Characterization of the flow regimes and the unsteady flow structures

4.2.2.1 Flow regimes

An example of wall shear rate courses measured inside the flow cell is shown in Fig.7.

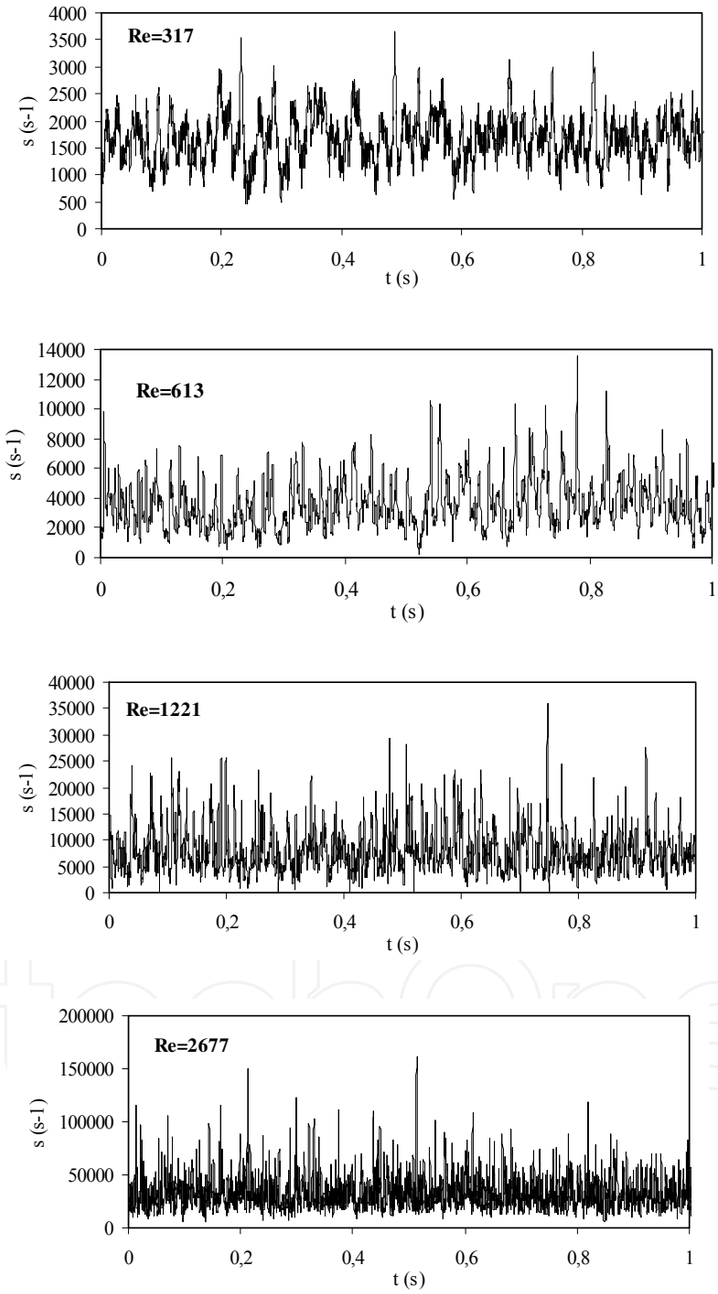

Fig. 7. Time-traces of the corrected wall shear rate recorded on electrode M15 for different Reynolds numbers

For these measurements carried out near the cell outlet, the first flow fluctuations are observed at the flow rate corresponding to Re~200. As the flow rate increases, the level of

fluctuations is enhanced and the wall shear rate reaches values which are higher than those observed in flow channels of common sizes.

It is interesting to analyze the results obtained for the microelectrodes located at the different axial positions. The study of fluctuation rates *FR*, which is presented in Figure 8, illustrates the typical flow regimes achieved in the flow cell and also the gradual evolution of fluctuations along the cell.

The variation of *FR* with *Re* is characterized by an initial plateau at *FR*~0 (laminar flow regime), then *FR* increases sharply (transient flow regime) up to a practically constant level (regime of developed flow fluctuations), whose actual value is depending on the specific probe location. The critical value of *Re* corresponding to the onset of fluctuations varies from 560 (for the probe M34 located close to the cell inlet) to 200 (for all the electrodes behind the third channel crossing). Therefore, the flow inside the network of channels can be considered as established for the axial locations of *X*>0.3.

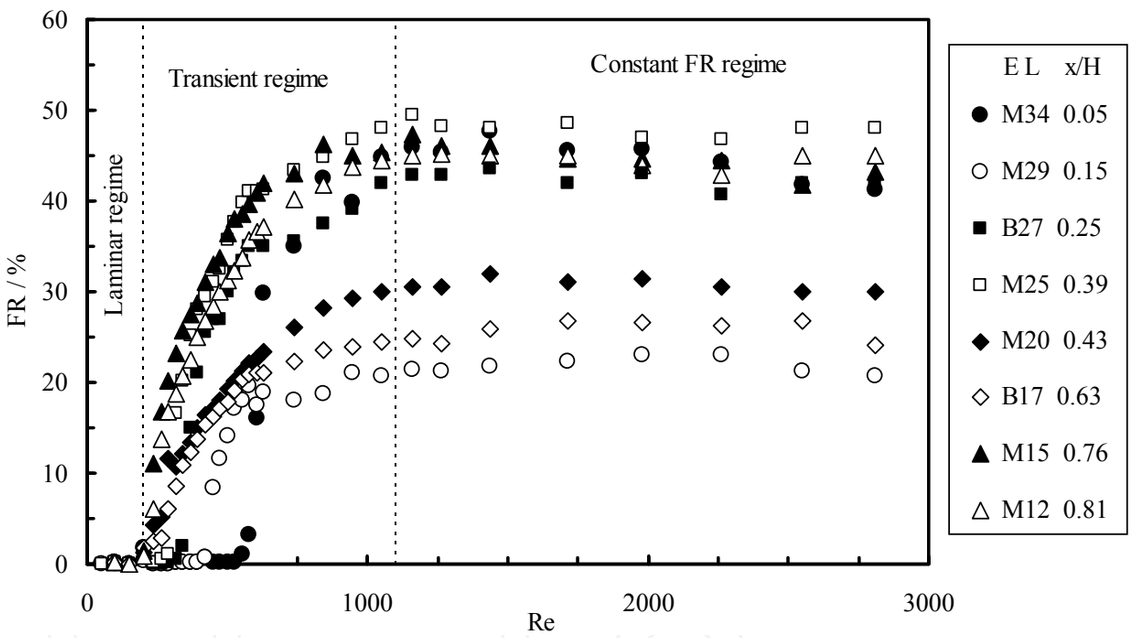

Fig. 8. Variations of fluctuation rates $FR = \sqrt{\overline{s'^2}}/\overline{s}$ with the Reynolds number obtained for the different axial locations $X=x/H$.

Only at low flow rates (for *Re*<200), the stable laminar regime is observed throughout the flow cell. On the other hand, the stabilization of near-wall flow fluctuations is reached at high flow rates and is observed anywhere in the cell for *Re*>1100. As the flow pattern is very complex (3D with recirculation zones behind the crossings), the final value of *FR* is very sensitive to the exact position of the microelectrode (especially with respect to the channel centerline). The fluctuation rates are found to stabilize at relative values ranging from 20 % to 50 %. The channel crossings have an effect on the enhancement of flow fluctuations and also on their earlier stabilization than in straight channels. The shape of *FR* versus *Re* curves is very similar to that observed for the evolution of fluctuations in packed beds of particles. The packed bed flow configurations exhibit also practically the same critical Re values

characterizing the onset (*Re*~180) (Seguin *et al*., 1998a) and the stabilization (*Re*~900) of flow fluctuations (Seguin *et al*., 1998b).

4.2.2.2 Flow structures

In complement to the preliminary interpretation regarding the flow structure by PIV (see section 4.1) analysis and wall shear stress measurements (Huchet *et al*., 2007), the wall turbulent eddies are classically assessed by the dimensionless autocorrelation of fluctuating velocity gradient and can then be calculated:

$$R_{ss}^{*} = \frac{R_{ss}}{R_{ss}(0)} \tag{21}$$

With

$$R_{ss}(t, dt) = \frac{s'(t)s'(t+dt)}{\sqrt{s'(t)^2}\sqrt{s'(t+dt)^2}} \tag{22}$$

Calculation of the autocorrelation provides information regarding the Taylor microscale, λ, and the integral length scale, Λ, by supposing the Taylor hypothesis, which is defined by:

$$\lambda = \tau_{\lambda} U_c \quad \text{with} \quad R_{ss}^{*}(t = \tau_{\lambda} \to 0) \tag{23}$$

Performing a Taylor series expansion of the autocorrelation $R_{ss}^{*}(t)$, the osculating parabola thus obtained is supposed to yield the derivative covariance:

$$R_{ss}^{*}(t = \tau_{\lambda}) = 1 - \frac{t^2}{{\tau_{\lambda}}^2} \tag{24}$$

The integral scale is given by:

$$\Lambda = U_c \int_0^{\infty} R^{*}_{ss}(t)dt \tag{25}$$

Integral length scales estimate the size of the largest turbulent eddies and can also be defined as the size of the large energy containing eddies, i.e. eddies containing most of the turbulent kinetic energy. Taylor microscale is a measurement of the dimension of eddies which transfer the kinetic energy at the scale of dissipation where the viscous phenomena predominate. The Taylor microscales represent the small-scale motion which are of significant interest in term of molecular mixing or micromixing.

In Figs. 9, the autocorrelation curve of the wall shear rate signals is plotted as a function of time at several locations between the inlet and the outlet of the network corresponding to the position of the microelectrodes in the minichannels.

It shows a large range of characteristic times corresponding to the convective time of the structures in the near location of the probes. Thus, the turbulence macroscales and microscales were calculated according to equations 15 and 14 for Re=2950 by using the Taylor hypothesis.

The sizes of the integral length scale, Λ, and the Taylor microscales, λ, are gathered in Table 2 according to their locations.

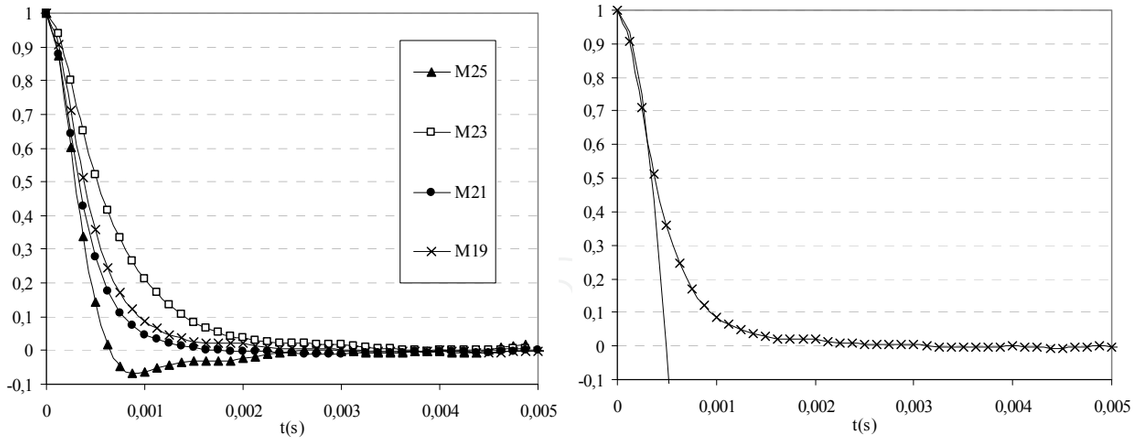

Fig. 9. Left: Dimensionless autocorrelation of the wall shear rate for different positions in the radial direction at X/H≈ 0.4 for *Re*=2950. Right: Autocorrelation function (solid line and crossing) at M19 location and osculating parabola (solid line) function (τ_λ=0.0005 s).

	Probes	*X/H*	*l/L/2*	τ_λ *(ms)*	λ *(mm)*	τ_Λ *(ms)*	**Λ (mm)**
Lateral evolution	M25	0.39	0.088	0.44	0.87	0.47	0.92
	M23	0.46	-0.959			3.32	6.54
	M21	0.43	-0.102	0.44	0.87	0.98	1.93
	M19	0.43	0.733	0.5	0.98	1.67	3.28
Axial evolution	M34	0.05	0.088	0.375	0.74	0.88	1.73
	M15	0.76	0.088	0.375	0.74	0.49	0.97
	M4	0.95	0.279	0.375	0.74	0.62	1.22
Crossing junction	C24	0.41	-0.008	0.44	0.87	0.81	1.59
	C14	0.79	-0.008	0.44	0.87	0.72	1.42
Before a crossing	B27	0.25	0.12	0.45	0.89	1.46	2.87
	B17	0.63	0.12	0.45	0.89	1.35	2.66
	B5	0.96	0.057	0.3	0.59		
After a crossing	A28	0.23	0.057	0.3	0.59	0.35	0.69
	A18	0.61	0.057	0.3	0.59	0.78	1.54

Table 2. Comparison of the macroscales and the Taylor microscales at different location in the network for Re=2950.

- Axial evolution
  The evolution between x/H=0.05 and x/H=0.95 at three locations (M34, M15 and M4) in the axial direction (0.088<z/(L/2)<0.279) is quite constant. The sizes of the Taylor microscale is equal to 0.74 mm and the sizes of the larger eddies is ranged between 0.97 mm and 1.73 mm which are of the same order of magnitude than the characteristic length of a square minichannel equal to 1.5 mm in side.

- Lateral evolution
  Regarding to the lateral evolution between z/(L/2)=-0.959 and z/(L/2)=0.733 at x/H ≈ 0.4, the results are scattered according to the position in the network. For M25 and M21 position, the sizes of the micro and macroscale respectively equal in average to 0.87 mm and 1.5 mm confirm the previous positions given that their location corresponding to the middle of the network (z/L/2 ≈ 0) and both to the middle of a channel.
  At the lateral positions of the network (M19 and M23) larger integral scales, respectively equal to 3.28 mm and 6.54 mm are observed.
  It corresponds to the length of a minichannel between two successive crossings equal to 5.5 mm involving that the shape of these larger vortices are spread out in the longitudinal direction and convected on average along the streamwise direction by the flow. At M23, the correlation coefficient presents a very restricted zone with a parabolic behaviour and can not satisfy the calculation of the Taylor microscale.
- At the channels crossings ("A, B, C" probes)
  In the crossing location, at a smaller scale, the Taylor microscales are of the same order of magnitude at the crossing junction and before the crossing ($\overline{\lambda} \approx 0.88$ mm) excepted for B5 position where a lower value is reported. This value is assumed to be due to the outlet effects which especially disturb the flow at this location. This particularity was already mentioned in the section 3.2 where the turbulent intensity field at the outlet is not representative of the remaining of the crossing flow inside the network.
  For microelectrodes located after the crossing (A), the low values of Taylor microscales ($\overline{\lambda} \approx 0.59$ mm) are maintained due to the recirculation zone observed by PIV.
  The sizes of the macroscales at "A" and "C" positions equal in average to 1.5 mm are lower than at position "B". In the first two locations, the sizes are controlled by the junction at the crossing involving the reduction of the flow section, while "A" position presents smaller turbulent scales induced by the recirculation zone. The mean size of the macroscales ($\overline{\lambda} \approx 2.77$ mm) found at the "B" position corresponds to the length between the crossing and the recirculation zone.

Finally, results regarding characteristic length scales of the turbulence (integral scales and Taylor microscales) show very different trends according to the geometry. Thus, from the PIV and electrochemical measurements, a general pattern describing the different scales inside a crossing of two minichannels transposable to the whole network of crossing minichannels in the constant fluctuations flow regime can be proposed. The integral scales are clearly dependent on the position in the network and particularly influenced by elbows and crossings.
In the present study, the confined geometry addicted by the crossing effects induces anisotropic spatial scales characteristics depending on the position in the channel and in the whole network.

4.2.2.3 Statistical flow properties

As seen in the previous section, the spatial heterogeneity of the flow structures need to investigate deeper the temporal anisotropy. Thus, statistics calculations are performed in order to characterize the hydrodynamics in term of degree of intermittency or anisotropy.
Experimental and numerical data dealing with intermittent turbulent flow are often characterized by statistical properties which are really different than in homogeneous and isotropic turbulence (Xu *et al.*, 2006; Portelli *et al.*, 2003). Most of the works concerning the study of the turbulent boundary layer has shown that this region is characterized by the

presence of ejection of coherent structures called "burst phenomena". These near-wall characteristics are linked by the presence of high velocity gradient and the measurements of the fluctuating quantities such as concentration or temperature are characterized by strong and rare fluctuations. In particular, the probability density function is deformed and the dimensionless fourth order moment, i.e. the flatness factor, F, is very different from the value 3 calculated in the case of Gaussian fluctuations. Moreover, the dimensionless third order moment, i.e. the skewness factor, S_k, can significantly increase above zero, which reveals intermittent and strong fluctuations. In the present work, we studied the small scales statistics issued of the electrochemical signals which are linked to the instantaneous limiting diffusion current. The fluctuations of the current correspond to the fluctuations of the concentration of the electrochemical species in the diffusion boundary layer.
Time-evolution of the fluctuating value of the wall shear rate measured at the location M15 is given in Fig. 7 for *Re*=2677. The temporal shifting around the mean value is the first criteria of the intermittency characteristics. More important positives fluctuations are noticed. The normalized histogram of the data at Re= 2950 is compared with a Gaussian distribution in the figure 10. It confirms the intermittency of the electrochemical signals characterized by an asymmetrical and non-Gaussian distribution of the fluctuations corresponding to a flatness factor of 8.3. Moreover, the skewness factor, S_k, which reveals the intensity of the fluctuations when its value is greater than 0, reaches 1.55 at this location.

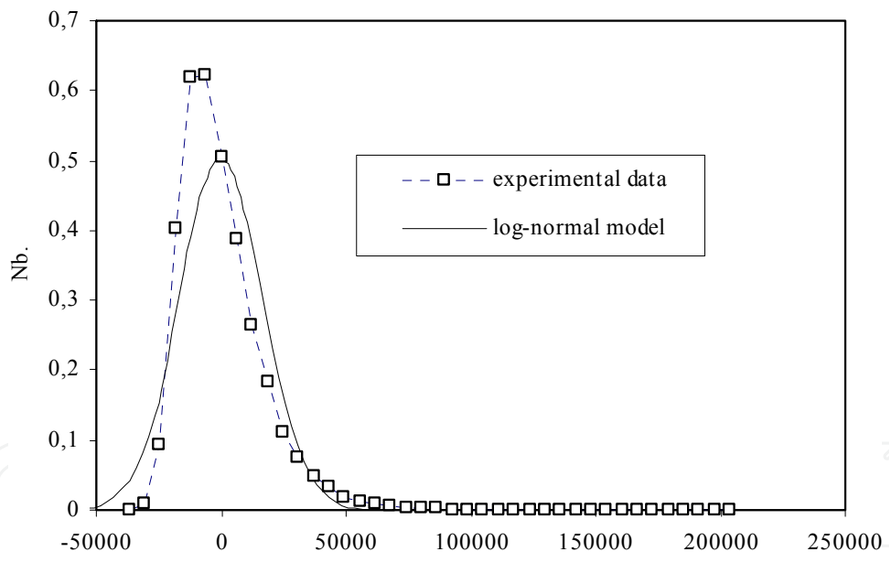

Fig. 10. Normalised distribution of the fluctuating wall shear rate at the location M15 for *Re*=2950 and comparison with a log-normal model.

For the purpose of our work, flatness and skewness factors are gathered in the Figure 11 for few locations corresponding to the positions of various microelectrodes. The calculation of the statistical properties of the electrochemical current have been performed by Adolphe *et al.* (2007) for transitional and turbulent straight channel flow which have described three different regimes such as:

- at Re<2000, in the laminar regime, the skewness values are $S_k \approx 0.3$ and flatness values are $F \approx 1.5$ revealing a range of fluctuations containing very low frequencies,

- for 2000<Re<4000, in the transient regime, the skewness factor is $S_k \approx 0.75$, which reveals the existence of strong and rare positive fluctuations associated with burst phenomena,
- in the turbulent regime (Re>10000), $S_k \approx 0$ and $F \approx 3$.

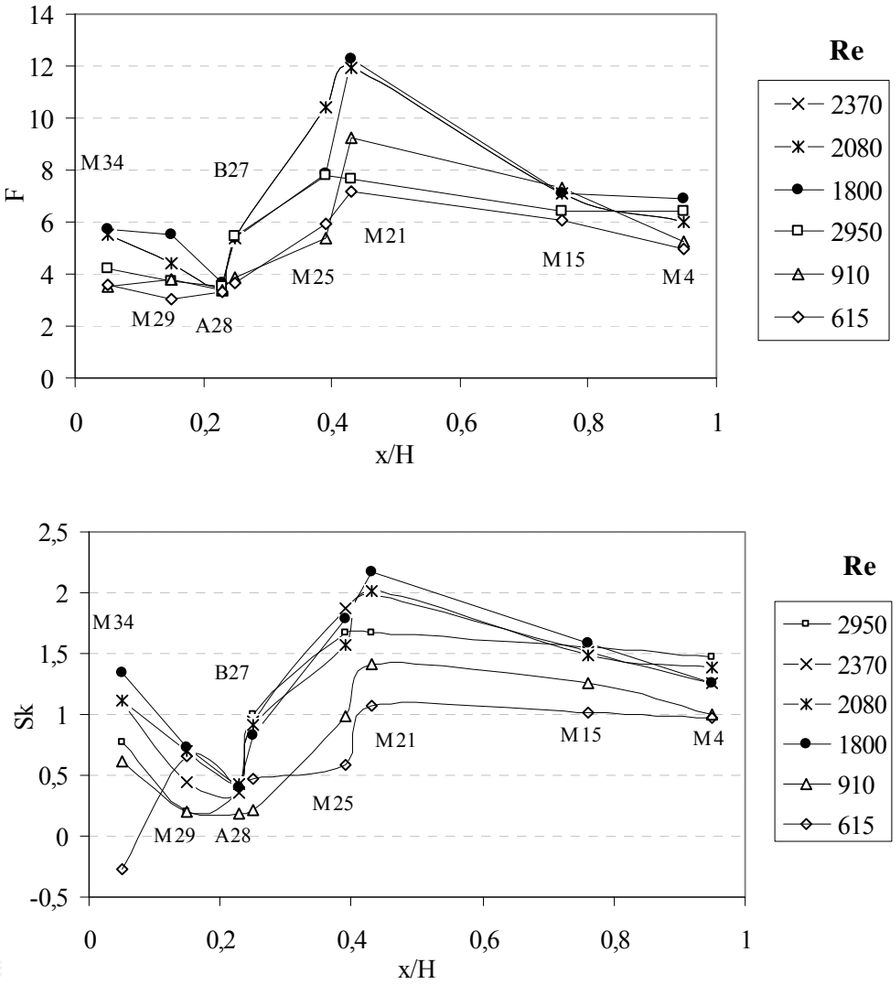

Fig. 11. Evolution of the flatness factor and the skewness factor in the network of crossing minichannels for various Reynolds numbers.

For most of the positions, the variation of F and S_k according to the Reynolds number are really different than in the straight channel configuration. Flatness factor varies between 3 and 11 until Re≈1800. From Re≈1800 to Re≈2800, the values decrease until to reach a constant value shifting between 5 and 8. The values of the skewness factor are ranged between 1 and 2 from the constant fluctuation flow regime (Re>1000). Thus, these statistical properties confirm a transient flow regime in the network of crossing minichannels. The transient flow regime is expanded above a Reynolds number equal to 1000 in spite of a constant fluctuation rate of the wall shear rate calculated by spectral analysis. Moreover, the fluctuations are noticeably stronger and the intermittent level is larger than in the case of a straight channel in transient regime.

In addition to the Reynolds number on the intermittency level, one can also notice about the influence of the axial location. The locations corresponding to the microelectrodes M29, A28 and B27 are characterized by lower values of the flatness and skewness factors. This zone (0<x/H<0.3) (section 4.2.2.1) is found as being the establishing length of the flow inside the network of crossing minichannels. The high values found at M34 are attributed to some inlet effects already mentionned in the PIV discussion in the section 3.2. At x/H≈0.4, the intermittency level rises and is found as be maximum at this location in the network whatever the Reynolds number considered. Beyond x/H≈0.4, the intermittency level is stable whatever the Reynolds number until the outlet (x/H≈0.95).
The statistical properties of the fluctuating values of the wall shear rate provide information regarding the intermittency characteristics of the flow in the near wall region at several locations inside the network of crossing minichannels. This statistical analysis allows us to verify the results discussed previously about the anisotropic scales observed by PIV inside a confined flow. Nevertheless, in the present case, it seems that the crossings could be also responsible of the intermittency by the decrease of the fluctuation rate of the wall shear rate at the junction.

5. Liquid-solid mass transfer and pressure drop characterization

5.1 Liquid-solid mass transfer

The experimental results on wall mass transfer obtained for three large electrodes are plotted in Figure 12.
These data are represented in the dimensionless form $ShSc^{1/3} = f(Re)$ by using the Sherwood ($Sh = k_{mt}dh/D$), Schmidt ($Sc=\nu/D$) and Reynolds numbers.
If the results are presented in logarithmic coordinates, two almost linear regions can be distinguished. Two corresponding correlations cover almost the whole range of experimental data:

$$ShSc^{-1/3} = 0.94\,\mathrm{Re}^{0.41} \tag{26}$$

(for 15<Re<100, in laminar regime)

$$ShSc^{-1/3} = 0.29\,\mathrm{Re}^{0.66} \tag{27}$$

(for 200<Re<3500, fluctuating regime)
The transition between these two mass transfer regimes is observed around Re≈100–200, i.e. at the flow rate for which the inception of near-wall flow fluctuations is expected. The mass transfer coefficient measured in the flow cell is significantly higher than that observed in straight square channels. As seen in Figure 12 the experimental data are clearly above the lines representing the Lévêque equation (Lévêque, 1928) (for laminar regime):

$$ShSc^{-1/3} = 1.85\left(\frac{d_h}{l_e}\right)^{1/3}\mathrm{Re}^{1/3} \tag{28}$$

and the equation obtained by the Chilton–Colburn analogy and cited by Coeuret & Storck (1984) (for turbulent regime):

$$ShSc^{-1/3} = 0.023\,\mathrm{Re}^{0.8} \tag{29}$$

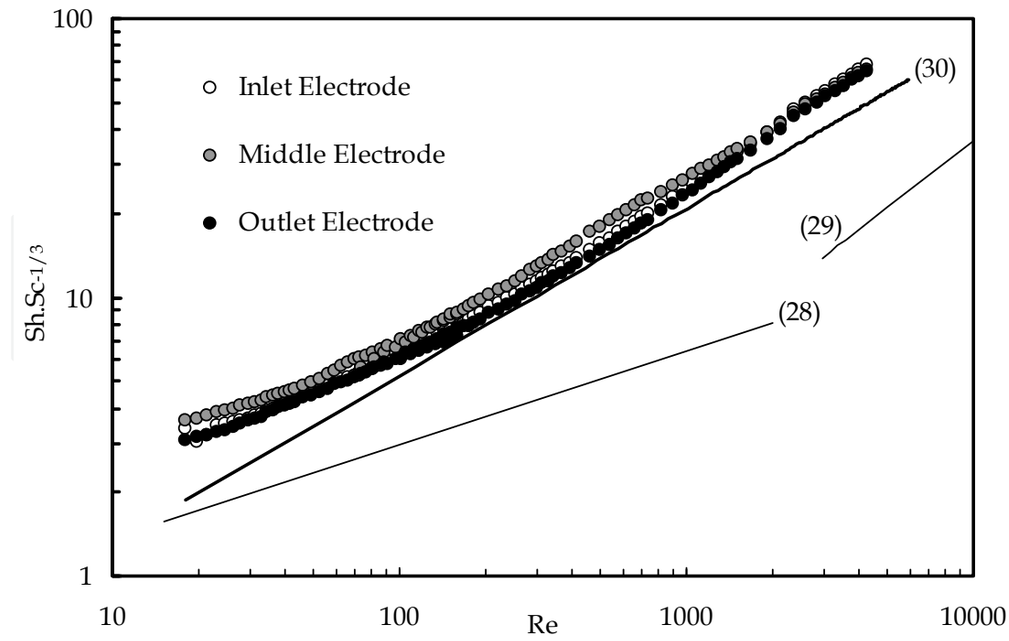

Fig. 12. Comparison of the measured wall mass transfer data with the correlation previously obtained for porous media and straight channels

For comparison, the classical correlation, which is proposed for mass transfer in fixed beds of spheres (Wakao & Funazkri, 1978), is also shown in Figure 12. After transformation of the particle dimensionless numbers into those for pore and application of the capillary model (Comiti & Renaud, 1989) for description of a microchannel network between individual spheres, the original Wakao correlation can be expressed in the form:

$$ShSc^{-1/3} = 1/3\,\mathrm{Re}^{0.6} \tag{30}$$

Where Re is identical to the Re_{pore}.
The analogy with a porous media takes into account three parameters. The specific surface, a_v, the porosity, ε, and the tortuosity, τ depend on the geometrical characteristics of the network such as represented in the figure 13:
a_v=1400 m^{-1} - ε=0,36

$$\tau = \frac{2(l + d_h)}{(l + d_h)\sqrt{2}} = \sqrt{2} \tag{31}$$

From the structural parameters from the capillary model, it is possible to determine the pore diameter of about 1.6 mm, close to the hydraulic diameter channels.
From the capillary representation of the network, the correlation of Wakao & Funazkri (1978) is, especially for Re>200, in relatively good agreement with the present mass transfer data (note the good agreement between the Reynolds number exponents in Equations 27 and 30). Consequently, from a mass transfer point of view, the studied flow cell can be compared to a porous medium rather than to a set of straight channels as demonstrated previously in the subsection 4.2.2.1 in the frame of the identification of the flow regimes from fluctuations rate of wall shear rate.

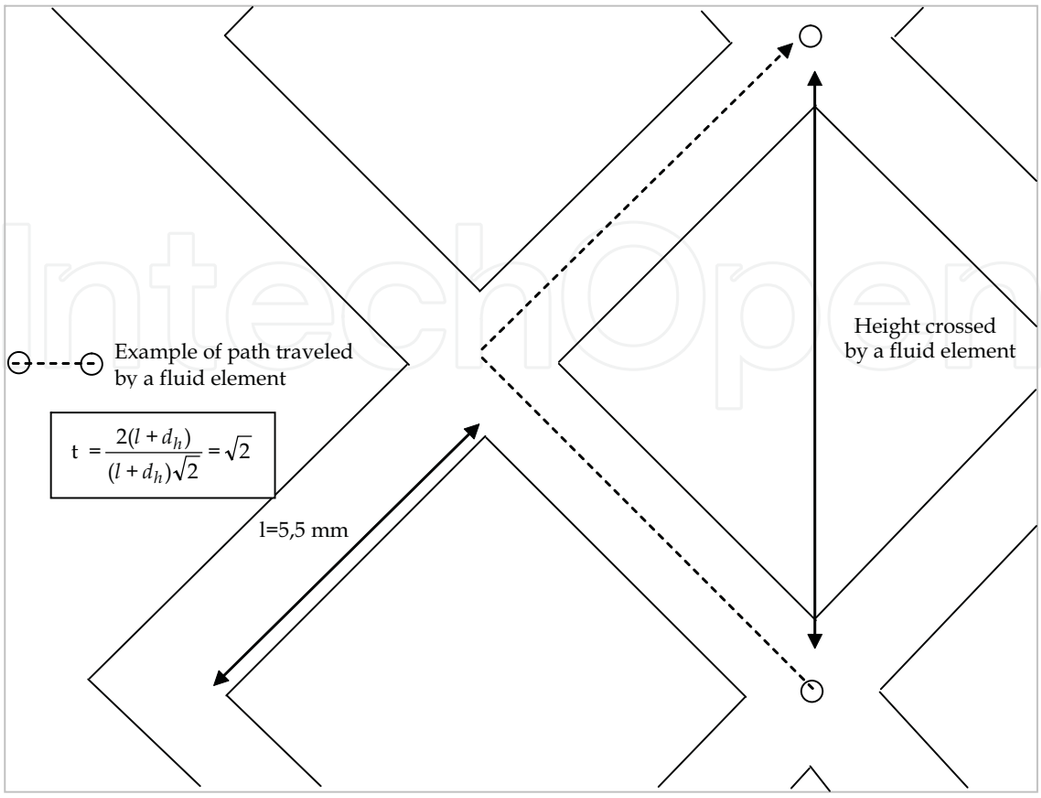

Fig. 13. Representation of motion of fluid particles used in calculating the tortuosity parameter through a capillary representation of the network of minichannels.

5.2 Pressure drop measurements

The measurements of pressure drop across the networks of height, H, are carried out by means of differential pressure valve located at the inlet and the outlet of the cell.

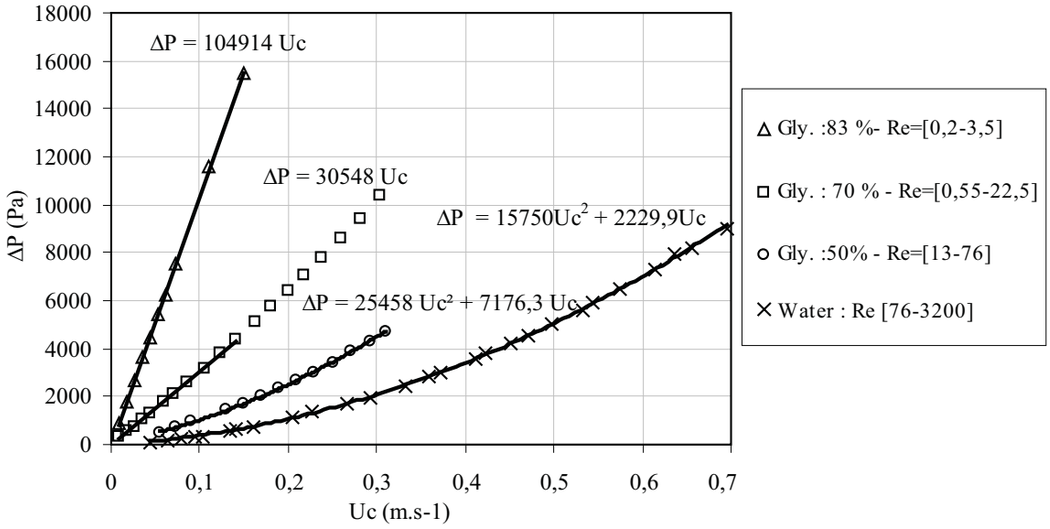

Fig. 14. Pressure drop as a function of the channel velocity for different liquids

The representation of the pressure drop as a function of the velocity is shown in Figure 14. Several aqueous solutions of glycerine are used in order to exhibit the linear part of the curve ΔP vs U_c and to identify the flow regime where the viscous force are preponderant.
The laminar flow regime can be divided in two parts:
-for Re<6~10, a linear part can be distinguished in the curves. This zone corresponds to a Reynolds number ranged between 0.5 and 10.
-for Re>10, a parabolic shape is representative of the pressure drop with a quadratic term similar to the Forchheimer type equation used for porous media:

$$\Delta P = M\eta U_0 + N\rho U_0^2 \tag{32}$$

Where U_0 is the superficial velocity, η the dynamic viscosity, and M and N depends on the porous medium structure.

6. Mixing performance in different networks of minichannels

We propose in the present section to use the electrochemical microsensors method in order to characterize the mixing performance in different geometries of network of minichannels.

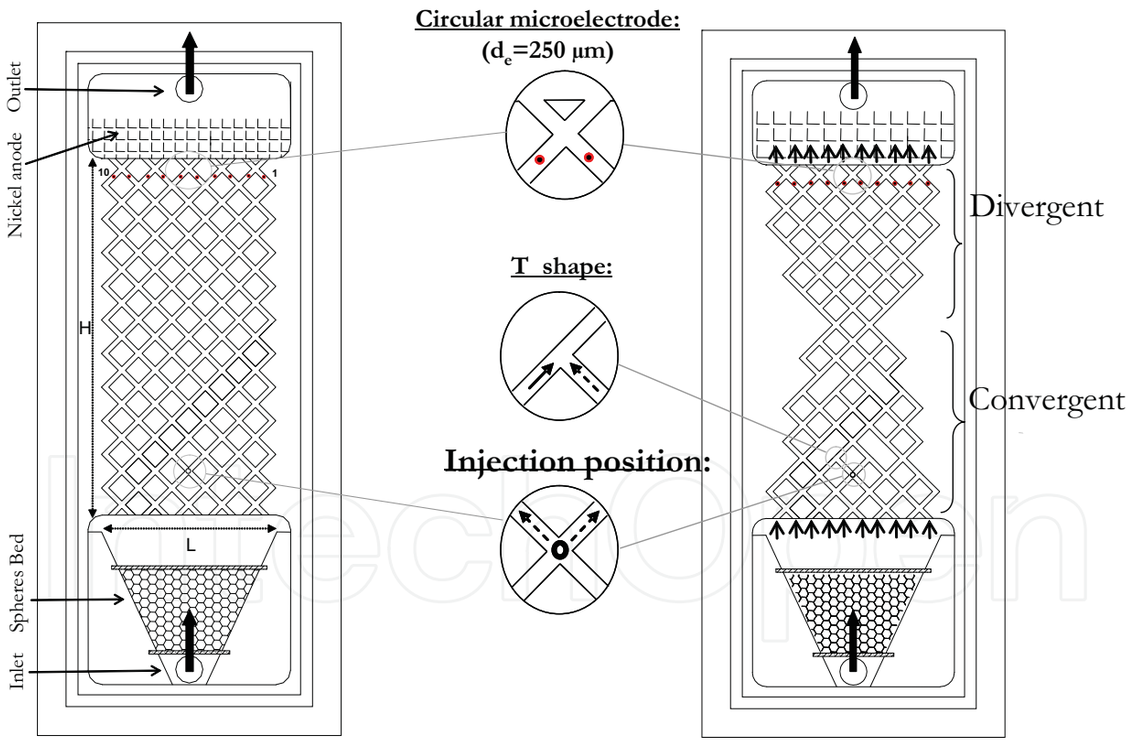

Fig. 15. Scheme of the experimental cells. Left: ×_network Right: T_network.

The working cells are presented in Fig. 15. One of them is the same network studied in the previous sections otherwise noticed ×_network. They are made in two altuglas plates and feature square minichannels in the upper plate. The second geometry, called T_network, corresponds to a better design for a mixing process.

The T_network is composed of a converging part in the first half of the cell followed by a diverging one in the remaining part of the network in order to induce a better distribution of the fluid until the outlet. The decrease of the flow section at the middle of the network reduces the distance between the streamlines and the path leading to the mixing process. Moreover, few T_shaped parts are integrated in the converging zone in order to enhance mixing.
The individual square-cross sections of the channels are the same either 1.5 mm in side. The whole test section has a length of H=105 mm and a width of L=52 mm. A third bottom plate is used for the two cells in order to perform electrochemical measurements. The location of the injection of the tracer in the flow cells is chosen at the second crossing in the median axis of the cells.
The limiting diffusion current on each microelectrode is registered at Reynolds numbers, Re, ranging from 50 to 250. The Reynolds number is based on the hydraulic diameter of the minichannels (d_h=1.5 mm) and the mean velocity inside an individual channel, U_c:

6.1 Measurements of the mixing level

6.1.1 Principle

The principle of mixing investigation is based on the simultaneous measurement of the limiting diffusion current at the channels outlets in order to quantify the mass amount of a tracer (the ferricyanide ions) injected upstream of the cells. The concentration of the electrochemical tracer, C_T, larger than the concentration in the electrochemical solution, C_0, flowing inside the cells is detected by the microelectrodes implemented at the wall of the ten outlet branches (from E1 to E10).
The network of crossing minichannels is primed by a minipump (Cole-Parmer Instrument) delivering a suitable electrochemical solution, kept at constant temperature (20 °C). The electrolyte is an aqueous solution of 0.002 M equimolar potassium ferro/ferricyanide and 0.057 M potassium sulphate working as supporting electrolyte. The physical properties of the solution are measured in the experimental conditions at constant temperature equal to 20 °C (ν=1.016×10^{-6} m^2.s^{-1}, D=7.98×10^{-10} m^2.s^{-1}). The electrochemical tracer is an aqueous solution of potassium ferricyanide of concentration, C_T, ranged between 0.025 and 0.15 M. Injection, realized at the second crossing minichannel after the inlet in the central axis of the network, is performed by using two methods:

- the first method is a pulse injection by using a syringe of volume equal to V_{inj} = 5.75 ml,
- the second method is a step injection by using a micro-pump (Armen instrument) delivering a constant flow rate equal to q_{inj} = 5 ml.min^{-1}.

All the experimental parameters are gathered in table 1. The ratio between Péclet and Reynolds numbers for the different investigated flow rates is greater than 1000, allowing to satisfy a forced convective flow regime.

Injection type	q_{inj} (ml.min^{-1})	V_{inj} (ml)	C_0 (mol.m^{-3})	C_T (mol.m^{-3})	U_c (m.s^{-1})	Re	Pe=$U_c d_h$/D
Pulse		5.75	2	25-50-100-150	0.038	57	75188
					0.076	114	144737
Step	5				0.107	161	204887
					0.165	247	313909

Table 3. Experimental parameters for the two methods of injection.

6.1.2 Mixing criteria

A home built electrodiffusion analyser is used to set the polarization voltage to the microelectrodes, to convert the simultaneously measured currents into voltages, and thus amplify the resulting signals. A polarization voltage of -0.8 V is applied to ensure limiting diffusional conditions. A PC controls the analyser operation and data recording. Data records (60000 samples) for 10 current signals are provided at a sampling frequency of 1 kHz.
Thus, at the beginning of recording, the injection of the electrochemical tracer is performed and examples of the signals recorded are shown in Fig 16 for the T_network in the case of the pulse injection and in the case of the step-shaped one for the ×_network. Others examples of recording of the limiting diffusion current are presented in the paper of Huchet *et al*. (2008)b.
From the measurements of the current intensity $I_i(t)$ obtained on each electrochemical sensor (i=1 to 10), the molar percentage of the tracer in each outlet minichannel is obtained, taking into account the base-line value, I_0, due to the limiting diffusion current induced by the bulk solution. Applying equation 2, one can write for the probe i:

$$\frac{\Delta C_i}{C_0} = \frac{C_i(t) - C_0}{C_0} = \frac{I_i(t) - I_{i0}}{I_{i0}} \tag{33}$$

$\Delta C_i(t)$ is the increase of concentration of ferricyanide ions on the probe i due to the tracer injection.
For the pulse injection, the molar percentage $\%n_i$ of the tracer in the outlet branch i is given by the following equation:

$$\%n_i = \frac{Q_c C_0 \int_0^\infty \left[\frac{I_i(t)}{I_{i0}} - 1 \right] dt}{\sum_{i=1}^{10} Q_c C_0 \int_0^\infty \left[\frac{I_i(t)}{I_{i0}} - 1 \right] dt} 100 = \frac{\int_0^\infty \left[\frac{I_i(t)}{I_{i0}} - 1 \right] dt}{\sum_{i=1}^{10} \int_0^\infty \left[\frac{I_i(t)}{I_{i0}} - 1 \right] dt} 100 \tag{34}$$

For the step-shaped injection, I_i and ΔC_i are constant:

$$\%n_i = \frac{Q_c C_0 \Delta C_i}{\sum_{i=1}^{10} Q_c C_0 \Delta C_i} 100 = \frac{\Delta C_i}{\sum_{i=1}^{10} \Delta C_i} 100 \tag{35}$$

Calculation of the molar percentage in each minichannel informs about the distribution of the tracer at the cells outlet. Thus, qualitative information is obtained regarding the mixing process inside the working systems.
In the other hand, a criterion of deviation is as well chosen in order to compare the mixing effectiveness for each geometry of minireactor. This is a classical criterion for evaluation of the mixing state. It compares the observed mixing with a perfect mixing state. In the present work, the measured molar percentage of the tracer is compared to a perfect distribution of the tracer which corresponds to a value of 10 % in the case of an ideal radial distribution. Thus, the mean relative deviation, σ, is given by:

$$\sigma = \sqrt{\sum_{i=1}^{10} (\%n_i - 10\%)^2 \Big/ 10} \tag{36}$$

The highest values of σ advise on poor performance in terms of mixing effectiveness and the smallest values of σ reveal a good degree of mixing.

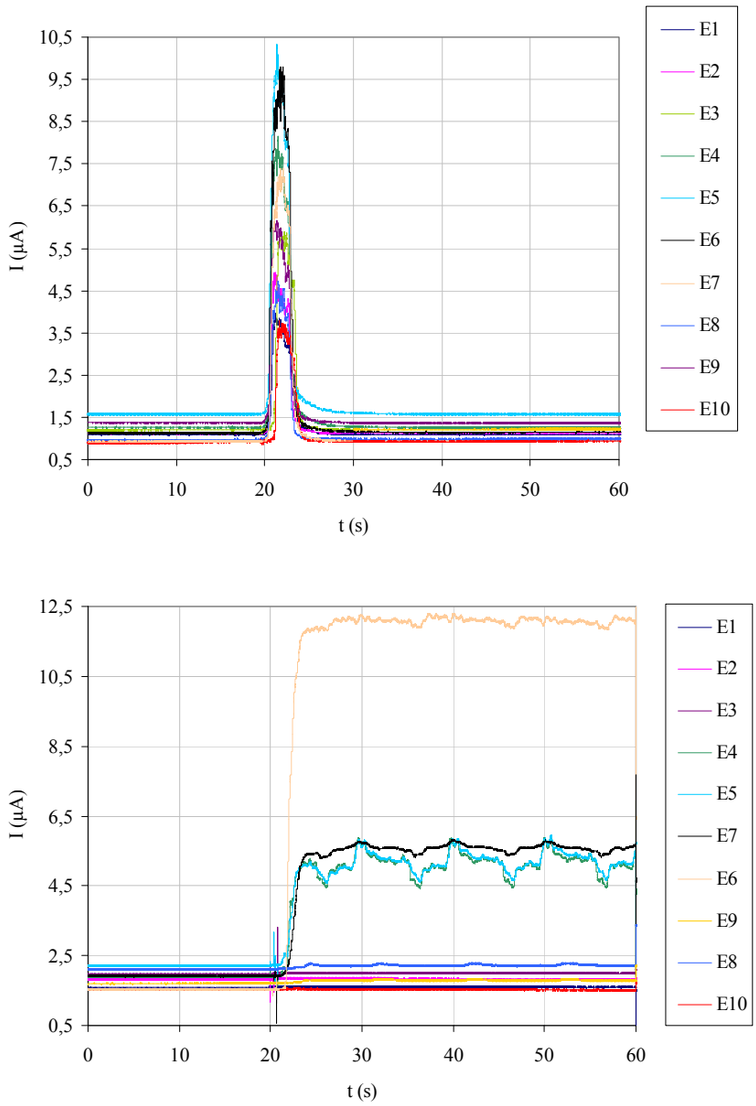

Fig. 16. Up : Time traces of the diffusion limiting current recorded during the pulse injection for the T_network. Down: Time traces of the diffusion limiting current recorded during the step-shaped injection for the ×_network.

6.2 Mixing performance of each network

6.2.1 Mixing quality

The radial distribution of the mass amount of tracer detected by the electrochemical sensors at the outlet of the two cells is presented in Figure 17 and 18 for Re=161 and C_T=50 mol.m^{-3}. The two injection techniques are representative of the tracer dispersion for each geometry of the cells. For the T_network, the radial dispersion is more important than in the ×_network and shows a better mixing state in this experimental condition.

Figures 19 and 20 synthesizes the whole experimental results which take into account the different tracer concentrations and the different Reynolds numbers studied. The relative deviation as a function of Reynolds number is plotted, emphasizing the preceding qualitative observation.

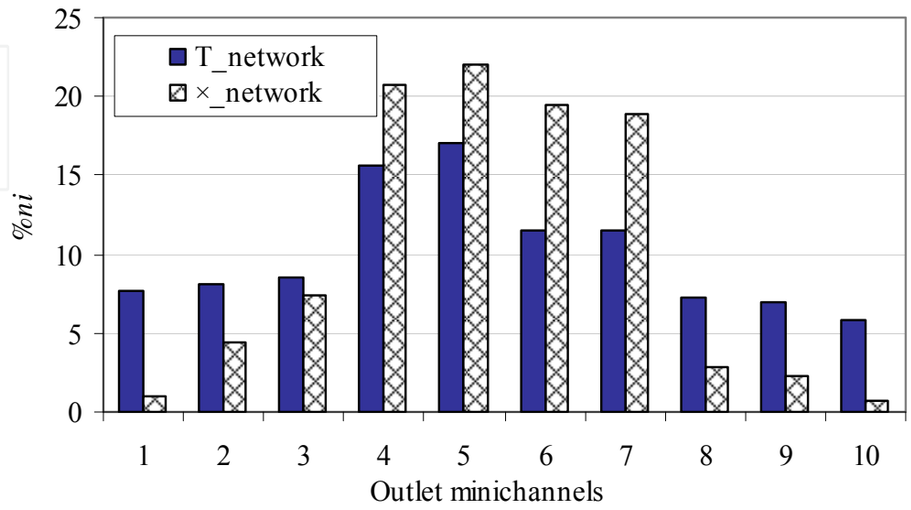

Fig. 17. Radial dispersion of the electrochemical tracer (C_T=50 mol.m^{-3}) at Re=160 for a pulse injection.

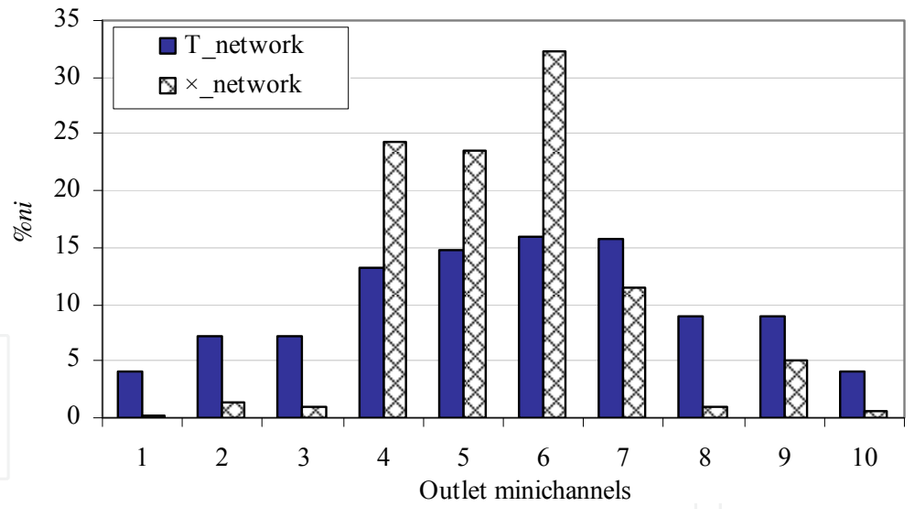

Fig. 18. Radial dispersion of the electrochemical tracer (C_T=50 mol.m^{-3}) at Re=160 for a step-shaped injection.

Except for *Re*≈57, the results reported in Fig. 20 show that the variances for the T_network are higher than for the ×_network, thus emphasizing a better effectiveness in terms of mixing whatever the Reynolds number. The zone of restriction between the convergent and the divergent contributes to decrease the path between the streamlines to force the mixing of the fluids. The values found at higher concentrations (C_T=100 mol.m^{-3} and C_T=150 mol.m^{-3}) for *Re*=57 are due to the dominating diffusion regime compared to the convective regime. Indeed, the concentration of the supporting electrolyte (K_2SO_4) is locally and briefly

decreased near the injection point. Furthermore, the pulse injection, especially for the small Reynolds number values induces a local increase of the flow rate due to the duration of the pulse injection which is not negligible compared to the entrance flow rate in the cell.

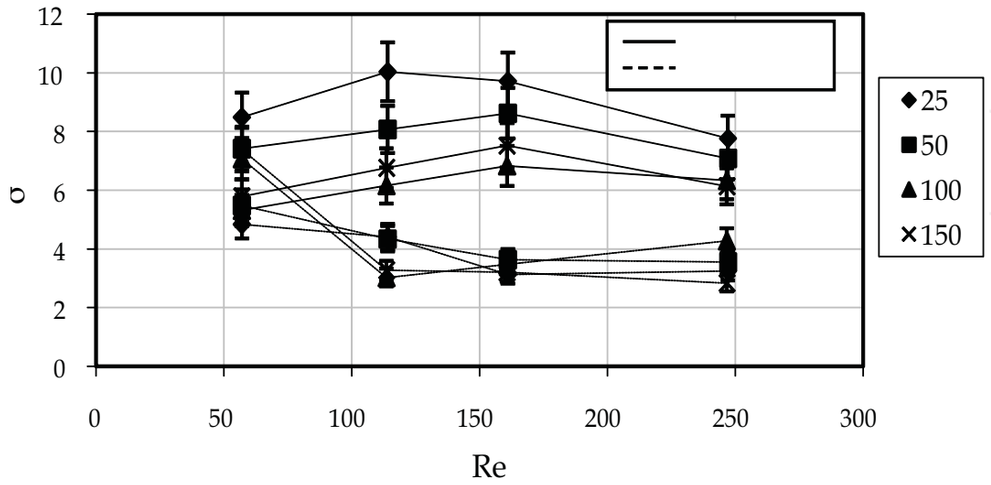

Fig. 19 Mixing effectiveness as a function of the Reynolds number at different lectrochemical tracer concentrations with the pulse injection method.

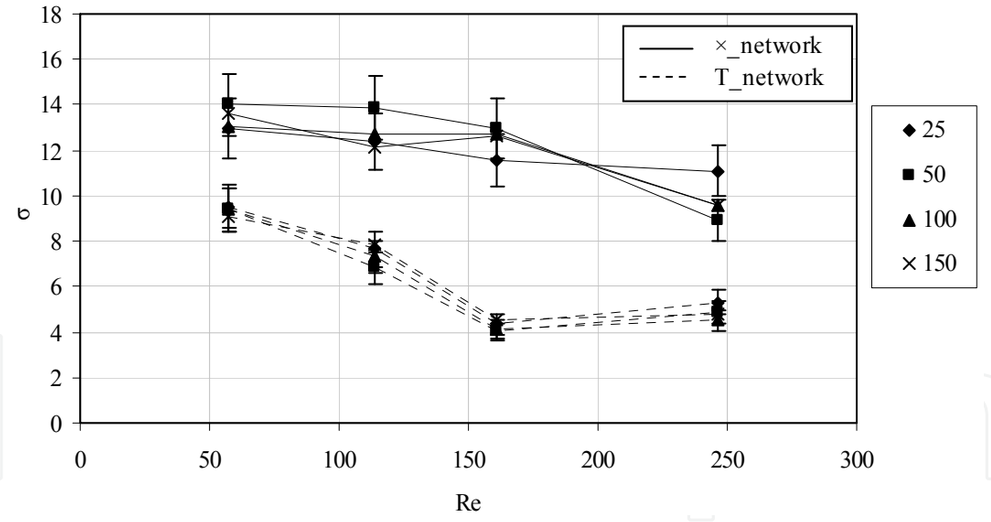

Fig. 20. Mixing effectiveness as a function of the Reynolds number at different electrochemical tracer concentrations with the step-shaped method.

For the step-shaped method (Fig. 20), the results confirm those previously obtained with the pulse method regarding the effectiveness of the mixing between the two geometries. Oppositely to the pulse injection, no dependence of the tracer's concentration is noticeable on the results for the two geometries. The results are not altered by the hydrodynamics generated by the injection, even at low Re values. The step-shaped technique can be considered as a better method in the mixing characterization for this kind of confined geometry.

For the ×_network, σ is found to be constant and equal in average to 13 until Re=161. Above Re=161, σ decreases to reach a value close to 10. This increase in terms of mixing performance is correlated to the first instabilities measured inside the network of crossing minichannels since the first fluctuations of the wall shear rate are quantified from Re≈200.
For the T_network, we observe a sharp decrease from Re≈57 until Re≈161. From Re≈161, σ is found to be constant at a value close to 4.5. This improvement of the mixing state is due to the geometry of the T_network inducing for a given flow rate several flow regimes in the network. For example, at Re≈114 at the inlet (calculation based on eq. 14), the Reynolds number varies in the channels from the converging zone until the restriction zone. At this last location for example, it remains only two channels for the fluid circulation and the velocity in each channel corresponds to a velocity equal to about 0.26 m.s^{-1}. Thus, the Reynolds number reaches a value equal to 400 at this position and thus contributes to the destabilization of the flow and an increase of the mixing capacity.

6.2.2 Energetic dissipation

The energy consumption of the working systems has to be evaluated in order to compare their efficiency as minimixer. Thus, measurements of pressure drop across the networks of height, H, are carried out by means of differential pressure valve located at the inlet and the outlet of the cells.

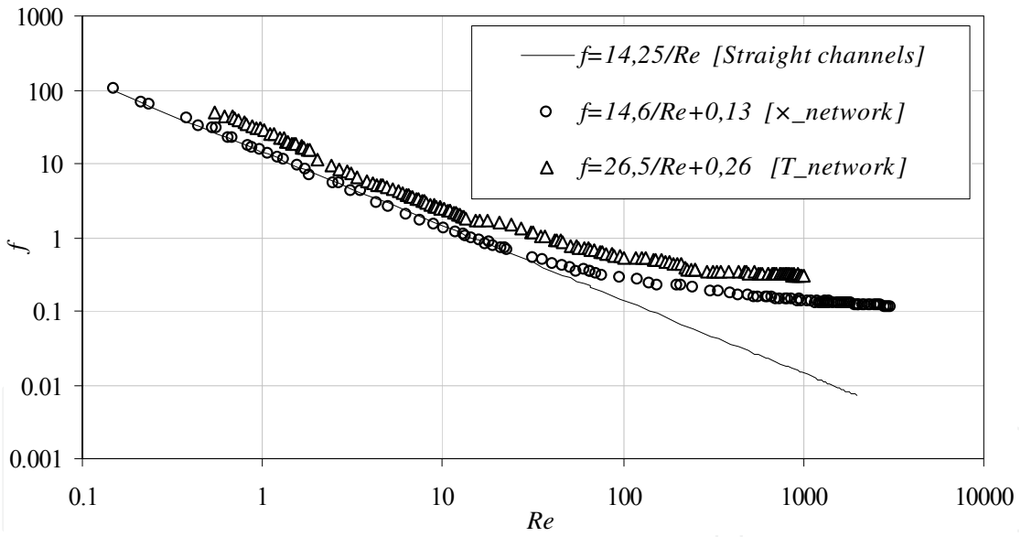

Fig. 21. Evolution of friction factor as a function of Reynolds number for the different geometries of network.

The experimental values of the pressure drop for all the used fluids and for all the Reynolds numbers are presented in Fig. 21 by using the friction coefficient, f, given by:

$$f = \frac{\Delta P}{H} \frac{d_h}{2\rho U_c^2} \tag{37}$$

This representation is useful to compare the different studied geometries (T_network and ×_network) with a set of ten straight parallel channels. Until Re≈10, the obtained values for

×_network and a set a straight channels are similar. For Re>10, an inertial contribution appears for the ×_network and the T_network due to the different shapes (crossing, bend or T_shaped).
It is important to notice that whatever the flow cell studied in the present work, the experimental results are quite well correlated by an equation of type:

$$f = \frac{A}{\mathrm{Re}} + B \tag{38}$$

With A=14.6 and B=0.13 in the ×_network case and A=26.5 and B=0.26 in the T_network. This equation, validated in a large range of Reynolds numbers (1<Re<1000) is similar to that employed in porous media confirming the analogy with the packed bed of particles proposed previously. For the T_network, the pressure drop is approximatively two times larger than for the ×_network for a given Reynolds number value. But T_network clearly ensures better mixing quality even at low Reynolds number, thus its use at lower Reynolds numbers allows energy saving for an identical or a better mixing quality. For example, in order to obtain the same mixing effectiveness corresponding to σ equal to about 9 (Fig.20: Re=55 for T_network, Re=250 for ×_network) it is necessary to bring 6 times more energy into the ×_network. From Re=114 in the T_network, the mixing performance increase to reach a value equal to 6 while the energy consumption remains 2 times less important than in the ×_network at Re=250.

7. Conclusion and outlooks

Hydrodynamics and mass transfer inside networks of minichannels of square section is studied by using different experimental techniques. Each technique is performed in order to characterize the flow and the mass transfer at several levels. Global measurements from pressure drop measurements and liquid-solid mass transfer has given a comprehensive approach and the comparison with known geometries from semi-empirical correlations. The local diagnostics of the flow is determined from Particle Image Velocimetry and electrodiffusional method in order to characterize the flow scales.
The main part of the research work has concerned a network of minichannels or so called ×_network. The sobolik's method was compared with the transfer function method from the assessment of the power density spectra (PSD) of the fluctuation of the wall shear rate. Shear rate fluctuations are observed for Re>200. Under transitional flow conditions, the fluctuation rate increases rapidly and reaches a locally constant level above a Reynolds number of about 1000. The onset and the stabilization of the wall shear rate fluctuations were found similar than those already measured in the porous media. Moreover, the flow is found to be laminar and the pressure drop governed by viscous dissipation only at low Reynolds number (Re<10). For Re>10 the flow regime remains laminar but the pressure drop is described by a Forcheimer type equation due to the kinetic energy degradation. A capillary model based on the geometrical parameter of the network (specific surface, porosity and tortuosity) has been used in order to compare the global liquid-solid mass transfer results with the correlation of Wakao & Funazkri (1978). It confirms that the network of crossing minichannels can rather be compared to a porous media than to a set of straight channels.

Mean velocity fields by PIV and wall shear rate fluctuations analysis from electrochemical microsensors have been focused in order to analyse the characteristic scales of the flow. PIV velocity data emphasize the developing behaviour of the flow between two successive crossings in the whole network. The inhomogeneous characteristics of the flow are confirmed by using wall electrochemical microsensors at different locations in the network. The wall turbulence eddies are studied by direct high frequency measurements of the wall shear rate. It shows unusually small scales characteristics: integral scales and Taylor microscales are relatively scattered and tend to be dependent on the cell geometry. Higher sizes of the integral scales are found in the lateral part than in the central one of the network. The contribution of the crossings as regards the size of the mixing eddies is less important in the lateral zone ($-0.73>z/L/2>0.96$) than in the axial zone ($-0.3<z/L/2<0.3$). The Taylor microscales are controlled by the confinement effects which induce a scattered spatial distribution between two successive crossings. This spatial heterogeneous distribution of the small scales is added to a temporal intermittency analysed by means of the statistical properties of the fluctuating wall shear rate quantities. We generally noted that the flatness and the skewness factors are respectively greater than 5 and greater than 1. Thus, the intermittency level is clearly larger than in the case of a straight channel in transient regime. The constant regime fluctuation defined from $Re\approx1000$ corresponds to a high level of intermittency which starts at $x/H\approx0.3$, is maximum at $x/H\approx0.4$ then reaches a stabilization beyond $x/H\approx0.4$.

Figure 22 summarizes the results from different methods inside this cell model.

The last item of the chapter has concerned the mixing performance characterization for two geometries of network: ×_network & T_network. Among the two tracer response techniques investigated (step-shaped and pulse), the results showed that the step-shaped method is more appropriated for a confined flow system. The diffusion-convective phenomenon at high concentration of tracer is limited due to a better hydrodynamics control at the injection location.

The results in the Reynolds numbers range, $55<Re<250$, concerning the T_network seem to be promising in terms of mixing effectiveness compared to the ×_network. In spite of pressure loss two times larger in the T_network than in the ×_network, it is possible to obtain the same or a better mixing effectiveness and to minimize energy consumption by working at clearly lower Reynolds number values in the T_network.

The results regarding the ×_network confirm preceding local hydrodynamics study and liquid-solid mass transfer measurements which exhibit similar behaviour than that observed in porous media in the Reynolds numbers range $1<Re<1000$. Evaluation of pressure drop in the T_network is as well represented by a Forchheimer equation as met in porous media.

The final ambition is to build some mixing model from these experimental data in one node of the network until the whole of the cell. It will help to design new microreactors with complex geometry (network of microchannels, porous media, constructal geometry). In other hand, some improvements of electrochemical microsensors are essential for characterization of transfer phenomena considering the high potential of this technique for the understanding of hydrodynamics and mass transfer phenomena inside the microsystems. Integration of double rectangular strip microelectrodes will inform about the directional characteristics of the wall-flow and the flow microscales in order to characterize the micromixing inside the mini and microreactors.

In conclusion, the flow inside Microsystems is generally not established with a predominant effect of the walls. The electrochemical method is the only one able to analyze developing unsteady flow characteristics in order to understand the unsteady phenomenology of ultra-confined flow developed inside micromixers and microreactors. Our next investigations are devoted in the mixing analysis inside different shapes of micromixers (Huchet *et al.*, 2008c)

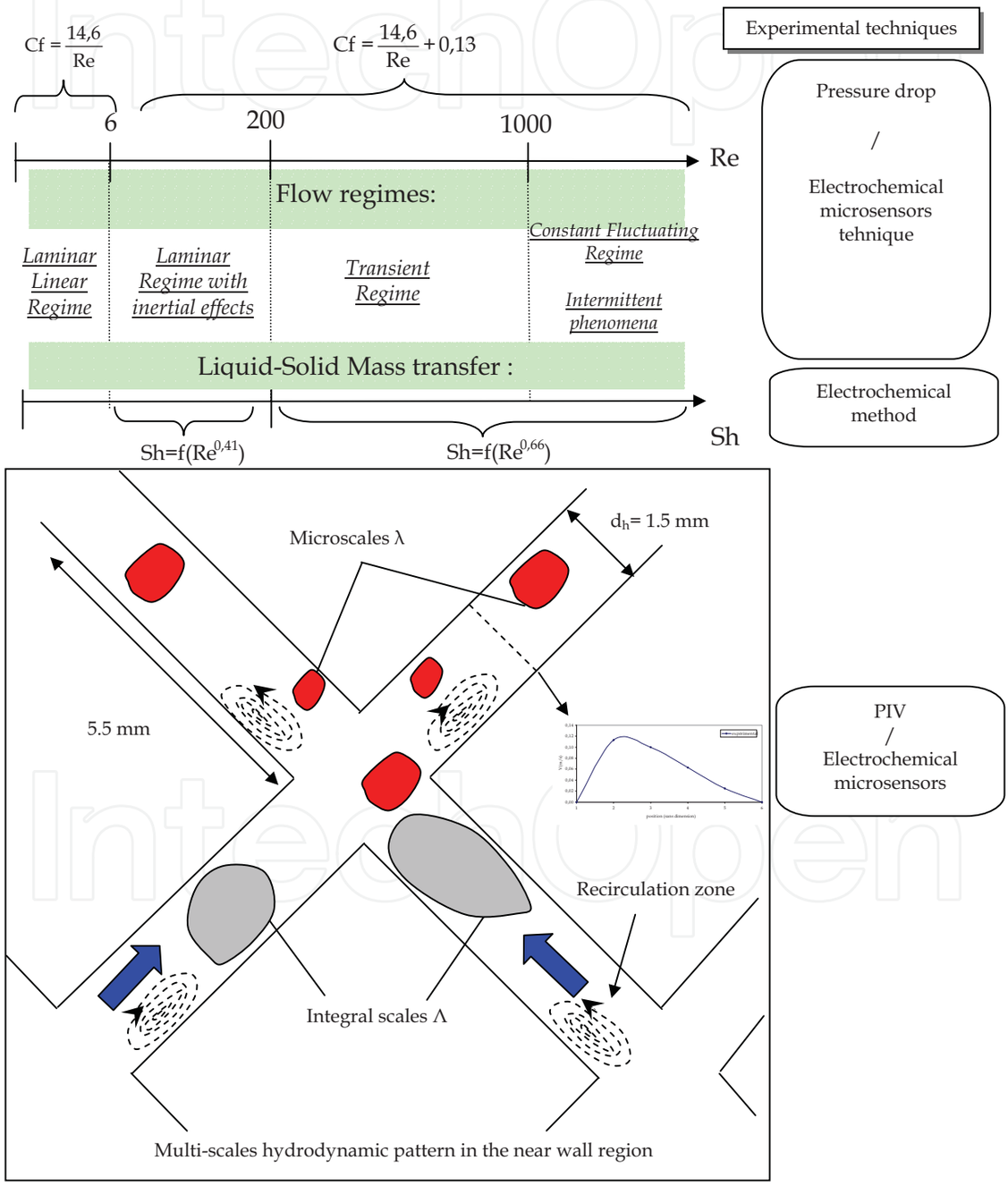

Fig. 22. Summary of results obtained from various experimental techniques in the ×_network

8. Acknowledgement

This work has been performed at the laboratory GEPEA –UMR CNRS 6144

9. References

Adolphe, X., Danaila, L. & Martemianov, S. (2007). On the small-scale statistics of turbulent mixing in electrochemical systems, *J. Electroanal. Chem.* 600: 119-130.

Bothe, D., Stemich, C. & Warnecke, H.J. (2006). Fluid mixing in a T-shaped micro-mixer, *Chem. Eng. Sci.* 61: 2950-2958.

Brandner, J.J., Anurjew, E., Bohnn, L., Hansjosten, E., Henning, T., Schygulla, U., Wenka, A. & Shubert, K. (2006). Concepts and realization of microstructure heat exchangers for enhanced heat transfer, *Exp. Therm. Fluid Sci.* 30: 801-809.

Coeuret, F. & Stork, A., (1984). *Eléments de génie électrochimique* Tec. Doc., Paris, 134-135.

Comiti, J. & Renaud, M. (1989). A new model for determining mean structure parameters of fixed beds from pressure drop measurements, *Chem. Eng. Sci*. 44: 1539-1545.

Commenge, J.M., Falk, L., Corriou, J.P. & M., Matlosz (2004). Intensification des procédés par microstructuration, *C. R. Physique* 5: 597-608.

Deslouis, C., Gil, O. & Tribollet, B. (1990). Frequency response of electrochemical sensors to hydrodynamic fluctuations, *J. Fluid Mech.* 215: 85-100.

Gunther, A., Jensen, K.F. (2006). Multiphase microfluidics: from flow, characteristics to chemical and materials synthesis, *Lab chip* 6: 1487-1503.

Hessel, V., Löwe, H. & Schönfeld, F. (2005). Micromixers - a review on passive and active mixing principles, *Chem. Eng. Sci.* 60: 2479-2501.

Lévêque, M.A. (1928). *Les lois de la transmission de la chaleur par convection*, Ann. Mines, Paris, 13: 201-239.

Hanratty, T.J. & Campbell, J.A. (1983). Measurement of wall shear stress in '*Fluid mechanics measurements*' (Eds.) J.R. Goldstein, Washington Hemisphere, 559.

Huchet, F., Comiti, J., Tihon, J., Montillet, A., & Legentilhomme, P. (2007). Electrodiffusion diagnostics of the flow and mass transfer inside a network of crossing minichannels, *J. App. Electrochem.* 37 1: 49-55.

Huchet, F., Legentilhomme, P., Comiti, J., Solliec, C., Legrand, J. & Montillet, A. (2008)a. Multi-scale analysis of near-wall turbulence intermittency inside a network of crossing minichannels by using electrochemical method and PIV measurements, *Int. J. Heat Fluid Flow* 29 5: 1411-1421.

Huchet, F., Comiti, J., Legentilhomme, P. & Bennadji, H. (2008)b. Mixing characterization and energetic dissipation in different networks of minichannels, *Chem. Eng. R. D.* 86 10A: 1135-1142.

Huchet, F., Havlica, J., Legentilhomme, P., Montillet, A., Comiti, J. & Tihon, J. (2008)c. Use of electrochemical microsensors for hydrodynamics study in crossing microchannels, Microfluid. Nanofluid. 5 1: 65-64.

Labraga, L., Lagraa, B., Mazouz, A. & Keirsbulck, L. (2002). Propagation of shear-layer structures in the near-wall region of a turbulent boundary layer, *Exp. Fluids* 33: 670-676.

Li, H. & Olsen, M. (2006). Examination of large-scale structures in turbulent microchannel flow, *Exp. Fluids* 40: 733-743.

Martemianov, S., Evdokimov, Y.K. & Adolphe, X. (2007). Electrodiffusion diagnostics of laminar flow using the delay-time method, J. Appl. Electrochem. 37: 1321-1328.

Max, J. (1985). *Méthodes et techniques de traitement du signal et applications aux mesures physiques*, ed. Masson, 4th edn.

Nakoryakov V. E., Budukov A. P., Kashinsky O. N. & Geshev P. I. (1986). Electrodiffusion method of investigation into the local structure of turbulent flows, ed. V.G. Gasenko, Novosibirsk.

Natrajan, V.K. & Christensen, K.T. (2007). Microscopic particle image velocimetry measurements of transition to turbulence in microscale capillaries, Exp. Fluids 43, 1-16.

Natrajan, V.K., Yamaguchi, E. & Christensen, K.T. (2007). Statistical and structural similarities between micro- and macroscale wall turbulence, Microfluid. Nanofluid. 3: 8-100.

Portelli, B., Holdsworth, P.C.W. & Pinton, J.F. (2003). Intermittency and non-Gaussian fluctuations of the global energy transfer in fully developed turbulence, *Phys. Rev. Lett.* 90 104501.1-104501.4.

Rehimi, F., Aloui, F., Ben Nasrallah, S., Doubliez, L. & Legrand, J. (2006). Inverse method for electrodiffusional diagnostics of flow, *Int. J. Heat Mass Transfer* 49: 1242-1254.

Reiss, L.P. & Hanratty, T.J. (1963). An experimental study of the unsteady nature of the viscous sublayer, *AIChE J.* 8: 154-160.

Sato, Y., Irisawa, G., Ishizuka, M., Hishida, K. & Maeda, M. (2003). Visualization of convective mixing in microchannel by fluorescence imaging, *Meas. Sci. Technol.* 14: 114-121.

Seguin, D., Montillet, A. & Comiti, J. (1998). Experimental characterization of flow regimes in various porous media-I: Limit of laminar flow regime, *Chem. Eng. Sci*. 53: 3751-3761.

Seguin, D., Montillet, A., Comiti, J. & Huet, F. (1998). Experimental characterization of flow regimes in various porous media II: Transition to turbulent regime, *Chem. Eng. Sci.* 53: 3897-3909.

Sobolik, V., Tihon, J., Wein, O. & Wichterle, K. (1998). Calibration of electrodiffusion friction probes using a voltage-step transient, *J. Appl. Electrochem*. 28: 329-335.

Sobolik, V., Wein, O. & Cermak, J. (1987). Simultaneous measurement of film thickness and wall shear stress in wavy flow of non-Newtonian liquids. *Coll. Czech Chem. Com.* 52: 913-928.

Tennekes, H. & Lumley, J.L. (1972). *A first course in turbulence*, Cambridge, MA: MIT Press, 8: 286.

Tihon, J., Tovchigrechko, V., Sobolik, V. & Wein, O. (2003). Electrodiffusion of the near-wall reversal in liquid films at the regime of solitary waves, *J. Appl. Electrochem*. 33: 577-587.

Wakao N. & Funazkri, T. (1978). Effect of fluid dispersion coefficients on particule-to-fluid mass transfer coefficients in packed beds. Correlation of Sherwood numbers, *Chem. Eng. Sci.*, 33, 1375-1384.

Wu, Z. & Nguyen, N. T. (2005). Hydrodynamic focusing in microchannels under consideration of diffusive dispersion: theories and experiments. *Sensors Actuators B* 107: 965-974.

Xu, C.X., Li, L., Cui, G.X. & Zhang, Z.S. (2006). Multi-scale analysis of near-wall turbulence intermittency. *J. Turbulence* 7: 1-15.

Yi, C., Zhang, Q., Li, C.W., Yang, J., Zhao, J. & Yang, M. (2006). Optical and electrochemical technique for cell based microfluidic systems, *Anal. Bioanal. Chem.* 384: 1259-1268.

IntechOpen

IntechOpen

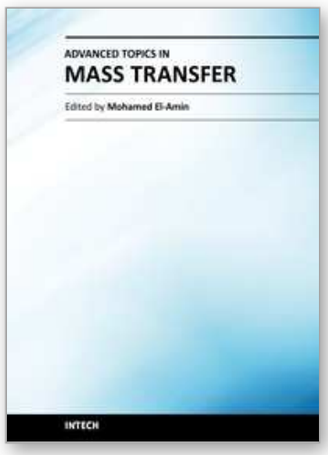

Advanced Topics in Mass Transfer

Edited by Prof. Mohamed El-Amin

ISBN 978-953-307-333-0
Hard cover, 626 pages
Publisher InTech
Published online 21, February, 2011
Published in print edition February, 2011

This book introduces a number of selected advanced topics in mass transfer phenomenon and covers its theoretical, numerical, modeling and experimental aspects. The 26 chapters of this book are divided into five parts. The first is devoted to the study of some problems of mass transfer in microchannels, turbulence, waves and plasma, while chapters regarding mass transfer with hydro-, magnetohydro- and electro- dynamics are collected in the second part. The third part deals with mass transfer in food, such as rice, cheese, fruits and vegetables, and the fourth focuses on mass transfer in some large-scale applications such as geomorphologic studies. The last part introduces several issues of combined heat and mass transfer phenomena. The book can be considered as a rich reference for researchers and engineers working in the field of mass transfer and its related topics.

How to reference

In order to correctly reference this scholarly work, feel free to copy and paste the following:

Florian Huchet (2011). Flow and Mass Transfer inside Networks of Minichannels, Advanced Topics in Mass Transfer, Prof. Mohamed El-Amin (Ed.), ISBN: 978-953-307-333-0, InTech, Available from: http://www.intechopen.com/books/advanced-topics-in-mass-transfer/flow-and-mass-transfer-inside-networks-of-minichannels

INTECH
open science | open minds

InTech Europe
University Campus STeP Ri
Slavka Krautzeka 83/A
51000 Rijeka, Croatia
Phone: +385 (51) 770 447
Fax: +385 (51) 686 166
www.intechopen.com

InTech China
Unit 405, Office Block, Hotel Equatorial Shanghai
No.65, Yan An Road (West), Shanghai, 200040, China
中国上海市延安西路65号上海国际贵都大饭店办公楼405单元
Phone: +86-21-62489820
Fax: +86-21-62489821

© 2011 The Author(s). Licensee IntechOpen. This chapter is distributed under the terms of the Creative Commons Attribution-NonCommercial-ShareAlike-3.0 License, which permits use, distribution and reproduction for non-commercial purposes, provided the original is properly cited and derivative works building on this content are distributed under the same license.

IntechOpen

IntechOpen